2022

Methodology to Treat Bottom Friction Losses for Modeling Wave Transformation From Deepwater to the Nearshore: An Application in Northeast Florida

Oscar Solisromero
University of North Florida, n01499003@unf.edu

METHODOLOGY TO TREAT BOTTOM FRICTION LOSSES FOR MODELING WAVE TRANSFORMATION FROM DEEPWATER TO THE NEARSHORE: AN APPLICATION IN NORTHEAST FLORIDA.

By

Oscar Solisromero

A Thesis submitted to the Department of Civil Engineering

in partial fulfillment of the requirements for the degree of

Master of Science in Civil Engineering

UNIVERSITY OF NORTH FLORIDA

COLLEGE OF COMPUTING, ENGINEERING AND CONSTRUCTION

December 2022

This Thesis titled “Methodology to treat bottom friction losses for modeling wave transformation from deepwater to the nearshore: An application in northeast Florida.” is approved:

Approved by the thesis committee: **Date**

_____ _____
William R. Dally, PhD, PE (Advisor, Committee Chair)

_____ _____
Dr. Raphael W. Crowley, PhD, PE (Committee Member)

_____ _____
Ryan Shamet, PhD, PE (Committee Member)

TABLE OF CONTENTS

LIST OF TABLES VIII

DEDICATION IX

ACKNOWLEDGEMENTS X

ABSTRACT XI

CHAPTER 1 INTRODUCTION, BACKGROUND, AND MOTIVATION 1

1.1 Introduction 1

1.2 Background 2

1.3 The Solution: Long-Term Nearshore 'Synthetic' Wave Records 3

1.4 Motivation 5

CHAPTER 2 STUDY AREA, DATA SOURCES, AND HINDCAST INFORMATION 6

2.1 The Region 6

2.2 The National Oceanic and Atmospheric Administration (NOAA): National Data Buoy Center (NDBC) Wave Record 8

2.3 NOAA Tides & Currents 9

CHAPTER 3 ADCP DESCRIPTION, DATA PROCESSING, AND DATA ANALYSIS 10

3.1 ADCP Description 10

3.1.1 Measured ADCP Data 11

3.1.2 Data Re-Processing and Analysis 12

CHAPTER 4 DEEPWATER HINDCAST INFORMATION 20

4.1 Why hindcast information? 20

4.2 Oceanweather, Inc. Deepwater Hindcast 21

4.3 Comparison of OWI-7611 Hindcast Results to NDBC-41112. 25

CHAPTER 5 DESCRIPTION OF STWAVE+ 31

5.1 STWAVE+ Spectral Wave Model. 31

5.2 Incorporation of Bed Friction: "STWAVE+" 33

5.3 STWAVE+ Modeling Structure and Procedure 34

5.3.1 Spectrum input (spec.in) 35

5.3.2 Bathymetry input (dep.in) 35

5.3.3 Bottom friction input (friction.in) 36

5.3.4 Options input (options.in) 36

CHAPTER 6 STWAVE+ GRID GENERATION 37

6.1 STWAVE+ Grid Boundaries and Bathymetry Generation 37

6.2 Global Multi-Resolution Topography (GMRT) 38

6.3 Surfer 42

CHAPTER 7 DEMONSTRATION OF THE CALIBRATION METHODOLOGY AND RESULTS 45

7.1 The Proposed Calibration Methodology 45

7.2 Computational Cost (Processing Time) 45

7.3 Results 46

7.4 Selection of the Best-Fit Friction Factor 47

CHAPTER 8 SUMMARY AND CONCLUSION 51

APPENDIX A OWI-7611 HINDCAST VS NDBC-41112 MEASURED TIME SERIES PLOTS FOR THE WAVE PARAMETERS FOR EACH MONTH 53

APPENDIX B 10-DAY SIGNIFICANT WAVE HEIGHT PLOTS: OWI-7611, NDBC (CDIP-132), AND ADCP PRESSURE & SURFACE TRACKING WITH INSTRUMENT AT 1M ELEVATION 59

REFERENCES 68

LIST OF FIGURES

Figure 2-1 a) Location of Buoy-41112 b) The buoy in its station (NOAA)..... 7

Figure 2-2 The study region. Measured data assets are indicated by red dots, whereas the locations of model-predicted information are indicated by black dots. 8

Figure 3-1 Teledyne-RD Instruments Workhorse Sentinel ADCP..... 10

Figure 3-2 ADCP mounted to a 3m stainless steel pipe water-jetted into the sea floor. 12

Figure 3-3 The main page of the WavesMon software during reprocessing of raw ADCP data. 13

Figure 3-4 WaveView display: Pressure tracking (WL) 'water level/depth'. Pressure transducer malfunction around January 19th, 2014. 16

Figure 3-5 WaveView display: Surface tracking (WL) 'water depth'. No malfunction on January 19th, 2014. 17

Figure 3-6 Comparison of 30-day moving average of the ADCP data with both configurations of surface tracking (in blue) and pressure tracking (in red), along with the measured tide gauge at Fernandina Beach (in black) and the tide predictions at the North Jetty (in green). 18

Figure 3-7 Comparison of pressure and surface tracking data with OWI and NDBC data. 19

Figure 4-1. The domain and associated grid of the GF-EC project (oceanweather, 2022) 22

Figure 4-2 - Water depths (0-500 m), referenced to mean sea level, in the domain of the GF-EC hindcast wave model (oceanweather, 2022)..... 23

Figure 4-3 – Locations of archived hindcast results and astronomic tide predictions (black dots), wave and water level measurements (red dots), and the boundary adopted for the STWAVE+ modeling. 25

Figure 4-4 Time-series comparison of wave parameters from the hindcast at OWI-7611 to the measurements at NDBC-41112. 28

Figure 4-5 Time series of OWI results versus NDBC measurements of significant wave height (Hs) during the entire eleven months the nearshore ADCP was deployed. 29
Figure 4-6 Scatter plot of significant wave height (Hs) for OWI-7611 vs NDBC-41112, for the entire eleven-month record. 30
Figure 5-1 STWAVE input and output files (Massey, Anderson, Smith, Gomez, & Jones, 2011). 34
Figure 6-1 Staggered mesh in STWAVE with the local coordinate (Massey et al., 2011) 37
Figure 6-2 Illustration of the multiple resolutions of the GMRT (Ryan et al., 2009).. 39
Figure 6-3 Grid download for the aimed location (Ryan et al., 2009)..... 41
Figure 6-4 Surfer dialog box display showing triangulation and linear interpolation. 43
Figure 6-5 Contour and color relief grid exported from Surfer. 44
Figure 7-1 STWAVE+ model output wave parameters..... 47
Figure 7-2 Scatter plots of half-plane STWAVE+ results for different values of Cf versus full-plane ADCP measurements. The solid black lines represent perfect agreement, and the red lines are linear best-fits. 48
Figure 7-3 Quantile-Quantile plots of half-plane STWAVE+ results for different values of Cf, versus full-plane ADCP measurements. 49

LIST OF TABLES

Table 4-1 – Location in latitude & longitude and Florida State Plane coordinates, distance from the shore, and the local mean water depth for each of the OWI hindcast nodes, the NDBC buoy, and the ADCP. 24

Table 4-2 Nomenclature for spectral parameters derived from the specific data. 26

Table 5-1 Range in friction factor (C_f), applicable for the bed stress model defined by Eq. 2, for various types of bed compositions..... 34

DEDICATION

This thesis is dedicated to my sons for their unconditional love and to my wife for her encouragement and support. Thank you.

ACKNOWLEDGEMENTS

I would first like to express my gratitude to my advisor, Dr. William Dally for his guidance, support, and assistance in accomplishing this thesis and throughout my graduate school journey. His help and support were of paramount importance to the completion of this work.

I would also like to thank Dr. Raphael Crowley and Dr. Ryan Shamet for being part of my committee. Your help and support with very tight deadlines, out-of-sequence work, and overall patience is immensely appreciated.

I also want to acknowledge my fellow classmates, Saeed Booshi and Camden Dean for their help and tutoring sessions. Also, my Matlab tutors, Dr. Ty Hesser and Frederick Soster; I would be completely lost without your patience and expertise in getting me up to an adequate level of proficiency with using Matlab.

ABSTRACT

Designers and other practitioners confront a wide range of problems in the coastal zone, which often require long-term nearshore wave data. However, such data are usually quite scarce. Consequently, either wave measurements from buoys deployed in deep water, or archived deepwater wave hindcast information, must be utilized by rigorous, physics-based transformation to the site of interest using one of many available numerical models. A main issue in conducting such an effort is accounting for losses in wave energy due to bottom friction, for which establishing a suitable bed friction coefficient (C_f) can be problematic. In the present study, a methodology is proposed in which a limited record of nearshore *in situ* measurements is used to guide the selection of an appropriate friction factor by using a combination of Quantile-Quantile (Q-Q) and "scatter-plot" techniques. The methodology is tested using 1) five months (July 2013 to December 2013) of directional wave measurements taken in the nearshore (~ 9m depth) off of Mayport, Florida, and 2) concurrent deepwater hindcast information that was archived at a location nominally 38 km off the coast (24.5m depth). The nearshore wave data were collected using an Acoustic Doppler Current Profiler (ADCP), and the deepwater hindcast information was developed and supplied by Oceanweather, Inc. A version of the well-known spectral wave transformation model "STWAVE", modified to include wave energy losses due to bed friction, is used to transform the deepwater hindcast record to the site of the nearshore wave gauge. By running the model across a range of friction factors for a single month of the wave record (October, 2013), the proposed calibration method is demonstrated and the most appropriate coefficient selected (C_f = 0.015 in this instance). The calibrated model is then run for the entire five months of ADCP record to validate the proposed methodology.

CHAPTER 1

Introduction, Background, and Motivation

1.1 Introduction

The "nearshore" is generally defined as the area between the coastline and the depth where waves cause sediment movement on the ocean floor (Dean & Dalrymple, 2004). Growing attention in the operational wave prediction community is focusing on the nearshore (Van der Westhuysen, 2012). This interest in wave research is partly due to the investigation of ocean waves as an energy resource due to its vast potential. This interest has also been accentuated due to increased sensitivity to coastal hazards and their associated impacts on coastal communities due to sea level rise and changes in storm patterns due to global climate change. (Janssen, Kleef, Mulder, & Tydeman, 2008).

From a coastal engineering perspective, nearshore wave information should be taken into consideration in the design of coastal structures such as piers, revetments, jetties, and breakwaters. Also, such data is an indispensable part of beach renourishment projects. Other applications include the development of sediment budgets for inlet and shoreline management, and the establishment of coastal construction control lines (CCCL).

Local wave measurements can be collected using a variety of instruments, but the most common are wave-riding surface buoys (based on accelerometer technology). However, these devices are usually placed in relatively deep water. Although these buoys can collect detailed wave energy frequency spectra, they can only provide rough estimates of wave direction. Although buoys can operate in shallow water, near-shore wave measurements technology has evolved from the use of a single pressure transducer (providing only a frequency spectrum) to a

combination pressure transducer and electromagnetic current meter (PUV). However, bottom-mounted pressure transducers cannot accurately resolve the higher frequencies of the wave spectrum and PUVs provide only a crude estimate of the directional distribution of wave energy. The measurement of directional wave spectra significantly improved with the development the Acoustic Doppler Current Profiler (ADCP) in the late 1990s, attributed to its ability (even when bottom-mounted) to range throughout the water column. The ADCP can measure fully directional spectra at high frequency and directional resolution. ADCP instruments also can measure water levels and vertical profiles of the mean current. Yet, if very long-term records are to be produced for nearshore waves, it generally must be done through numerical modeling, using long-term wave data available from deepwater wave buoys, or from wave hindcast models. In general, due to wave energy losses due to friction with the ocean floor, the accurate transformation of offshore wave data/hindcast results to the nearshore is heavily dependent on 1) the specific model/algorithm adopted, and 2) the bed friction factor selected, which varies depending on the bed composition (*e.g.* mud, sand, rock, or coral). In other words, the fundamental issue confronting the practitioner is, for the friction model being used, to establish the value of the friction coefficient, C_f, that will provide the most accurate results when the waves reach the nearshore.

1.2 Background

Several notable efforts have been made in the past to collect continuous long-term *in situ* wave data in the nearshore regions of the United States using the various instruments described above. The Coastal Data Information Program (CDIP), operated by the University of California, San Diego, began collecting wave data off the coast of California in the 1970s using surface

buoys, and now operates many buoys on the east, west, and Gulf of Gulf of Mexico coasts of the U.S. However, most buoys are in water deeper than fifteen meters, and therefore their measurements are generally not appropriate for direct use in the nearshore.

The Florida Coastal Data Network (FCDN), operated by the University of Florida, deployed a series of bottom-mounted pressure transducers and PUV gauges throughout the Florida coast. By 1980, six units had been installed by FCDN, and two more were proposed to be installed later. Some of them collected data for as much as three years (Howell, 1980). The U.S. Army Corps of Engineers (USACE) deployed a linear array of fifteen pressure transducers along the 8-meter-deep contour at the Field Research Facility in Duck, North Carolina (Pena, 2019). Despite a large gap in the record from February 2012 to June 2016, this remains the longest record of coastal wave data in existence. The Florida Institute of Technology started a coastal wave data collection program in 1996 at Sebastian Inlet, Florida. This started with the PUV system and switched to an ADCP in the early 2000s. However, there are large gaps in the early wave record, especially in winter. Finally, Surfbreak Engineering Sciences, Inc. installed and maintained an ADCP wave measurement station near the coast (at depth 8.5m and 615m from the beach) at Melbourne Beach, Florida. The station operated for over 10 years from August 2001 to November 2011, with a data-capture rate of 94 percent (Leadon, Dally, & Osiecki, 2004).

1.3 The Solution: Long-Term Nearshore ‘Synthetic’ Wave Records

As discussed above, long-term real-time nearshore wave measurements are very rare, and even these records tend to contain significant gaps. In addition, there are very few locations where such data are available. Because gaining the necessary insight would otherwise require recording data for dozens of years, it is evident that a reliable alternative is needed. Due to this

lack of measured coastal wave data, 'synthetic' coastal wave information is usually produced by transforming 'hindcast' archived deep-sea waves into shallow water at the location of interest. The quality of extracted nearshore wave data based upon the deep-water records depends on several factors: 1) the reliability/validity of the model used to generate the deep-water hindcast, 2) the reliability/validity of the wave model used to transform the deep-water waves to the nearshore, and 3) the reliability of the bathymetry used by the nearshore wave transformation model.

Since every wave model has its specific representations for the physics of water waves, its associated assumptions, and adopts a particular numerical procedure, the outputs of different wave models often differ significantly in their attempt to provide a solution to what is usually a complicated simulation. Since coastal wave information is not yet generated using a standard procedure, both wave hindcasting methods and transformation models are still being developed and refined by researchers. The Florida Coastal Forcing Project (FCFP) attempted to address these issues by developing a consistent methodology for creating nearshore synthetic wave records along the Florida coast, described by William R Dally and Osiecki (2006). Concisely, the idea is to exploit available deepwater hindcast results and accurately transform it to shallow nearshore waters. This is because despite being artificial, deepwater hindcasts come with some advantages. They are generally l) available in sufficiently long records, 2) validated to available measurements from the many deepwater buoys as well as, more recently, satellite data, 3) available as fully directional spectra, and 4) consistently derived and continuous records. “Bringing the waves” from deep water to shallow water requires a transformation model. However, due to the various compositions of the sea floor, the wave transformation model must

be locally calibrated for energy losses due to bed friction, depending on a limited amount of *in situ* measured nearshore wave data.

1.4 Motivation

The purpose of this work is to develop, validate, and provide the coastal engineering community with a reliable and utilitarian methodology for calibrating the wave transformation models used in the development of nearshore synthetic wave records, based on methods developed by William R Dally and Osiecki (2006). This methodology was applied to a deepwater wave hindcast for Northeast, Florida, specifically the Mayport region. After discussing why Mayport was chosen for this effort in Chapter 2, ADCP description and its data processing and analysis is discussed in Chapter 3. Chapter 4 is the source of long-term deep-water hindcast information. In Chapter 5, the proposed methodology for using a limited amount of nearshore measurements to calibrate STWAVE+ for wave energy losses is presented. Chapter 6 discusses the grid generation to run the STWAVE+ model. In Chapter 7 the calibration methodology and results are demonstrated.

CHAPTER 2

Study Area, Data Sources, and Hindcast Information

2.1 The Region

The region selected for this study lies adjacent to the northeast coast of Florida, as shown in Figure 2.1. This area was chosen because on July 2, 2013, a bottom-mounted ADCP was installed by personnel from the University of North Florida, approximately 3000m offshore of the open-coast beach of Naval Station Mayport, Florida, in nominally 9 m water depth, as located in the figure. The instrument was deployed in "self-record" mode for a total of eleven (11) months, during which measurements of directional wave spectra, water levels, and current profiles were collected. Due to its record length and location in the nearshore, this relatively unique data record was expected to be well-suited for application of the friction-calibration methodology.

Other valuable measured-data assets available in this particular study area include concurrent directional wave measurements from the National Data Buoy Center (NDBC) Buoy #41112 (NDBC-41112), shown in Figure 2-1, offshore of St. Mary's Entrance to Kings Bay, Georgia, as well as concurrent water level measurements from NOAA tide gauge #8720030 located in Fernandina Beach, Florida. Note that in Figure 2.1, the locations of *measured* assets are indicated as red dots.

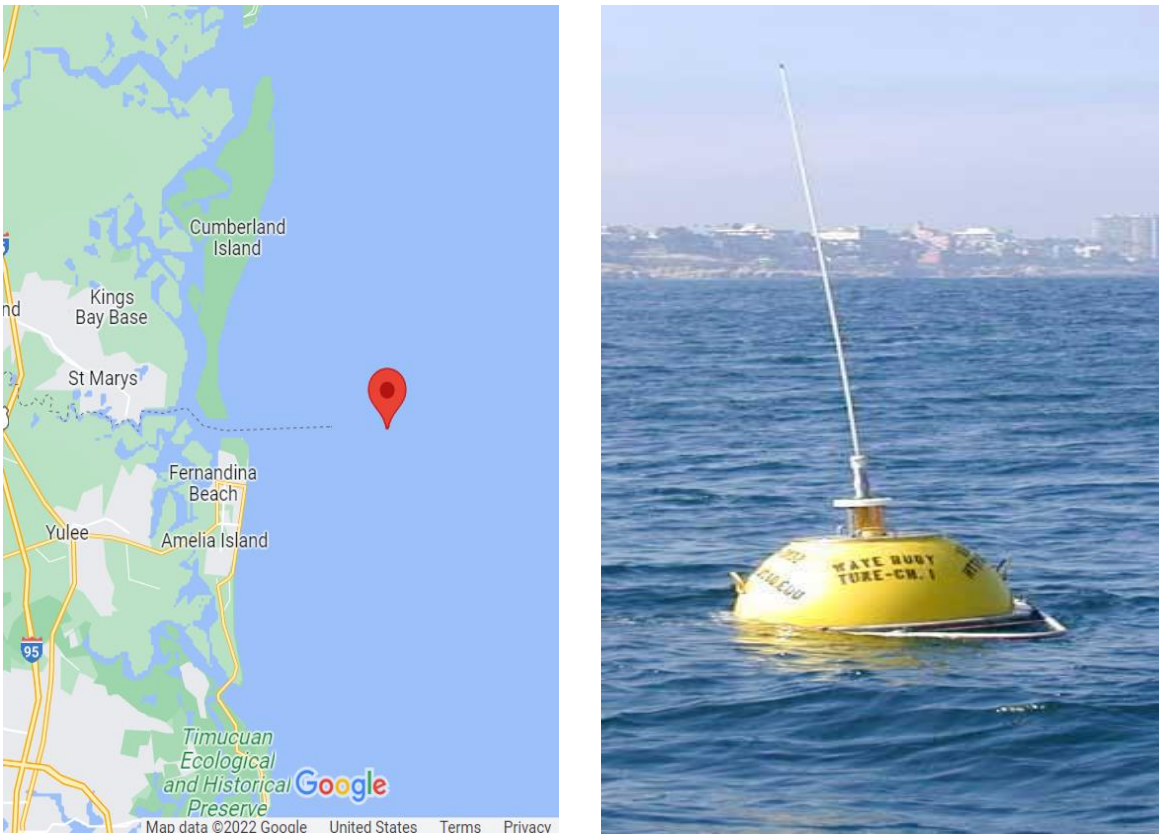

(a) (b)

Figure 2-1 a) Location of Buoy-41112 b) The buoy in its station (NOAA)

The locations of the *predicted/modelled* assets described below are indicated by black dots, and include five nodes (7611, 7198, 7130, 7062, 7203) from a commercial deepwater wave-hindcast product called "GROW-FINE" developed by Oceanweather, Inc. and kindly provided to the author. Also indicated in Figure 2.1 is a NOAA tide-prediction station #8679997 located adjacent to the north jetty of St. Mary's Entrance.

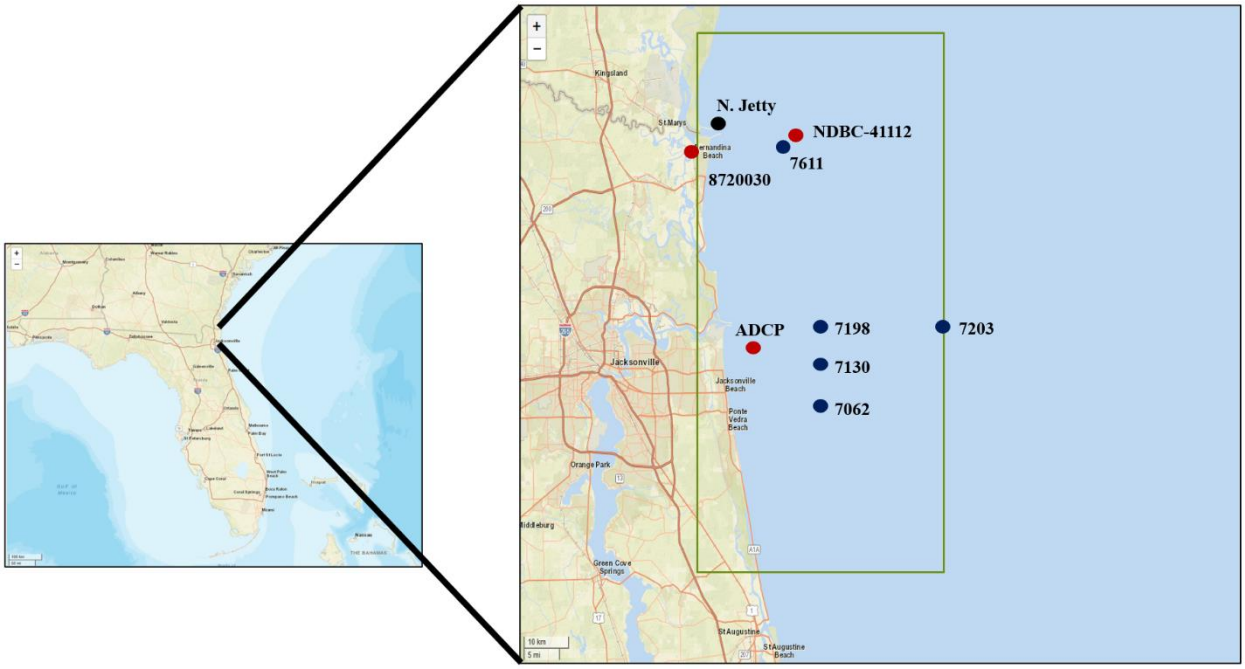

Figure 2-2 The study region. Measured data assets are indicated by red dots, whereas the locations of model-predicted information are indicated by black dots.

2.2 The National Oceanic and Atmospheric Administration (NOAA): National Data Buoy Center (NDBC) Wave Record

The National Data Buoy Center (NDBC) is a part of the National Oceanic and Atmospheric Administration's (NOAA) National Weather Service (NWS). NDBC designs, develops, operates, and maintains a network of data collecting buoys that measure and archive directional wave spectra, as well as report wave parameters such as wave height, wave period, and wave direction every 30 or 60 minutes. NDBC also operates Coastal Marine Automated Network (C-MAN) stations, which measure wind speed, direction, and other meteorologic phenomena. NDBC-41112 is a waverider buoy located at 30.71°N, 81.29°W at a nominal depth

of 16 m (51 ft). As described in detail in section 2.1, in this study NDBC-41112 was utilized to check the veracity of the wave hindcast results from the nearby GROW-FINE node #7611.

2.3 NOAA Tides & Currents

The Fernandina tide gauge, located inside the bay, provides real-time *measurements* of local water level, updated every six (6) minutes, whereas the tide *predictions* made at the North Jetty are representative of the ocean tide. Both the tide gauge at Fernandina Beach (8720030) and the tidal predictions at the North Jetty (8679997) were utilized in identifying and troubleshooting the water level measurements reported by the ADCP when its pressure transducer malfunctioned, to establish the correct time datum, and to track instrument elevation when reprocessing the raw data from the ADCP.

CHAPTER 3

ADCP Description, Data Processing, and Data Analysis

3.1 ADCP Description

Acoustic Doppler Current Profiler (ADCP) is an acoustic device with an arrangement of typically three or four transducers (Figure 4-1), which transform electrical to acoustic energy to measure the waves, currents, and water levels (Simpson, 2001). The fundamental assumption of ADCP technology is that sound-reflecting scatterers, such as plankton and detritus, move at the same speed and direction as the local water (R. D. Instruments, 1996).

Figure 3-1 Teledyne-RD Instruments Workhorse Sentinel ADCP.

In overview, a bottom-mounted, up-looking ADCP captures measurements of the time-dependent fluid speed and direction throughout the water column above. The ADCP measurements are based on the Doppler shift principle, which states that if a source of sound is moving relative to the sound receiver, there will be a shift between the transmitted and the

received sound frequency. The frequency of the acoustic energy transmitted by an ADCP transducer is shifted once when received by the scatterers, and a second time when received by the ADCP. Thus, the speed and direction of the water along the acoustic beam, p, is calculated as (Gordon, 1996):

$$p = \frac{c(f_B - f_s)}{2f_s} \quad (1)$$

in which c, f_B, f_S denote the speed of sound in water, sound frequency backscattered from the particles, and sound frequency transmitted from the ADCP transducer, respectively. The location of the measured water velocity along an acoustic beam is determined based on the time required for the backscattered signal to return to the ADCP.

3.1.1 Measured ADCP Data

In the present study, the data collected by the ADCP installed from July 2, 2013 to May 30, 2014 off of Naval Station Mayport, Florida were utilized. The ADCP was installed atop a 3m-long (10ft) stainless steel pipe. The pipe was water-jetted into the sea floor which penetrated the bed to the extent that the instrument head was nominally 1m (3.3ft) above the sea floor (see Figure 4-2). This ADCP, collected eleven months of nearshore directional wave data.

Figure 3-2 ADCP mounted to a 3m stainless steel pipe water-jetted into the sea floor.

3.1.2 Data Re-Processing and Analysis

The raw data collected by the ADCP were re-processed using the program "WavesMon" which is available from the instrument manufacturer, Teledyne RD Instruments. A screenshot taken during a typical execution of WavesMon is presented in Figure 3-3.

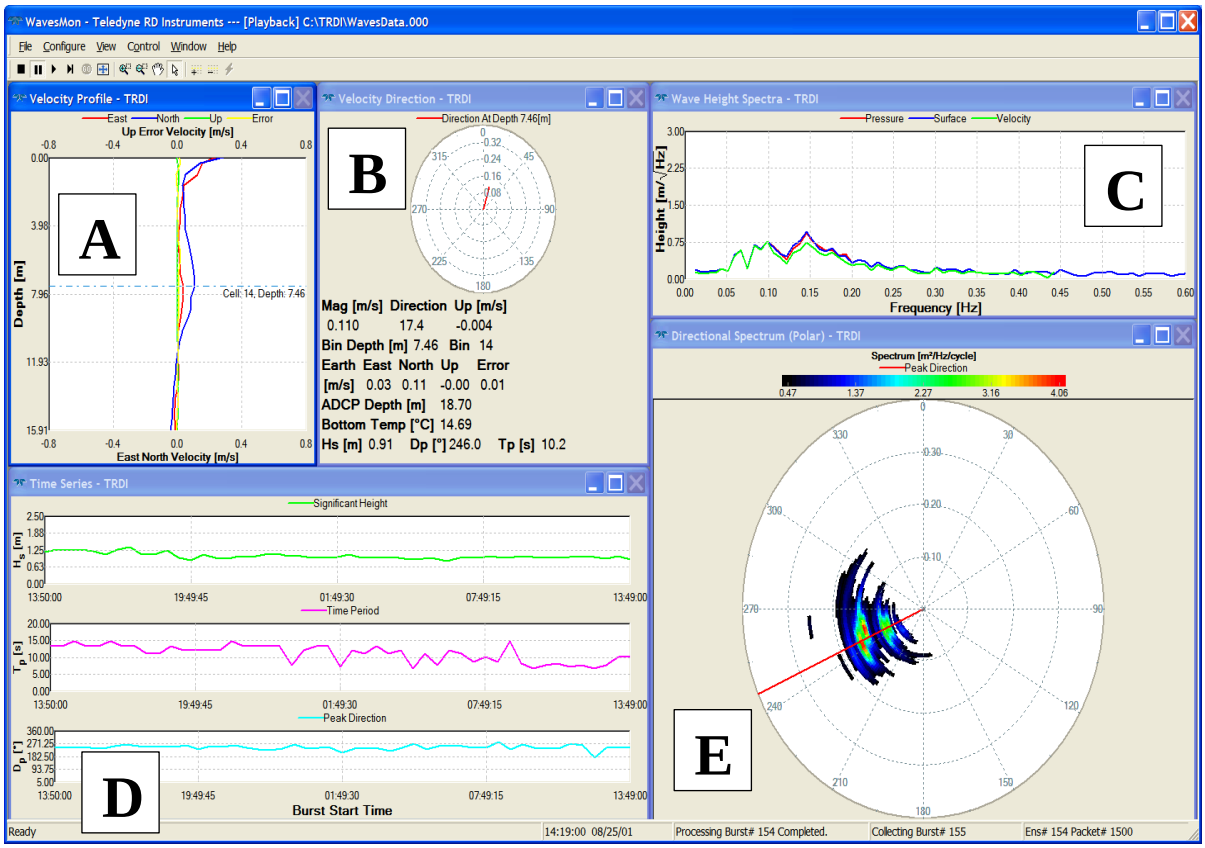

Figure 3-3 The main page of the WavesMon software during reprocessing of raw ADCP data.

There are five main displays when operating WavesMon and are detailed below as A-E:

A. Velocity Profile Plot: The profile view displays a current profile in the coordinate frame in which it is to be gathered by the ADCP.

B. Current Velocity Direction: This view displays the current magnitude and direction with an analog line. The length of the line is scaled the same as the scale selected for the profile plot.

C. Wave Height Spectra: The wave height spectra view displays height spectra in units of $[\frac{m}{\sqrt{Hz}}]$ as calculated from the pressure sensor, orbital velocities, and surface echo location.

D. Time Series: The time series window displays time series of significant wave height, peak period, and peak direction.

E. Directional Spectrum Polar: The default scale is set to dynamic. Red is maximum and black is minimum.

This software utilizes the Doppler-shift-derived, along-beam velocities from three upper layers of the water column as detected by the four transducers, as if there were a suspended array of twelve "virtual" current meters. The fundamental assumption of WavesMon is that there is a relation between the auto- and cross-spectra of the velocity series, computed from the returns of the individual acoustic beams. Then, the Iterative Maximum Likelihood Method is applied to calculate a high-resolution directional wave spectrum that closely agrees with the auto- and cross-spectra of the measured velocities (Churchill, Plueddemann, & Faluotico, 2006). With this technique, waves from, *e.g.*, two distinct directions such as sea and swell, can be separately identified, and even reflected waves resolved.

Data processed by WavesMon can then be plotted using "WavesView" software. This software enables the user to examine the time series of wave parameters and frequency and direction spectra, in seeking, for example significant changes or events (R. Instruments, 2008). In other words, WaveView provides the user with the "big picture" of the wave time series, and enables them to assess significant wave height, peak period, peak direction, and water depth.

Two examples of the WaveView displays for water level/depth (WL) are shown and discussed in detail in the following section.

However, sometimes an ADCP may return questionable results – especially in the context of using bottom-mounted pressure measurements to infer water election. Figure 3-4 and Figure 3-5 produced using WaveView to display water level (WL) of the re-processed ADCP data for the present study. In Figure 3-4, pressure tracking was selected as the primary source for configuring the water level. As it can be seen in this figure, the water level was measured as expected from the launch date in July until about mid-November. However, starting in early November, the water level started to rising to over 10.5m, that was around one meter higher than that of previous months. There was a second anomaly that occurred on January 19th, 2014 when the water level jumped dramatically to over 12m depth and then trended downward over the next few months until the end of the study. These "jumps" in the data are likely an error due to with the pressure transducer atop of the instrument which can become clogged with fine sediment and cause a malfunction.

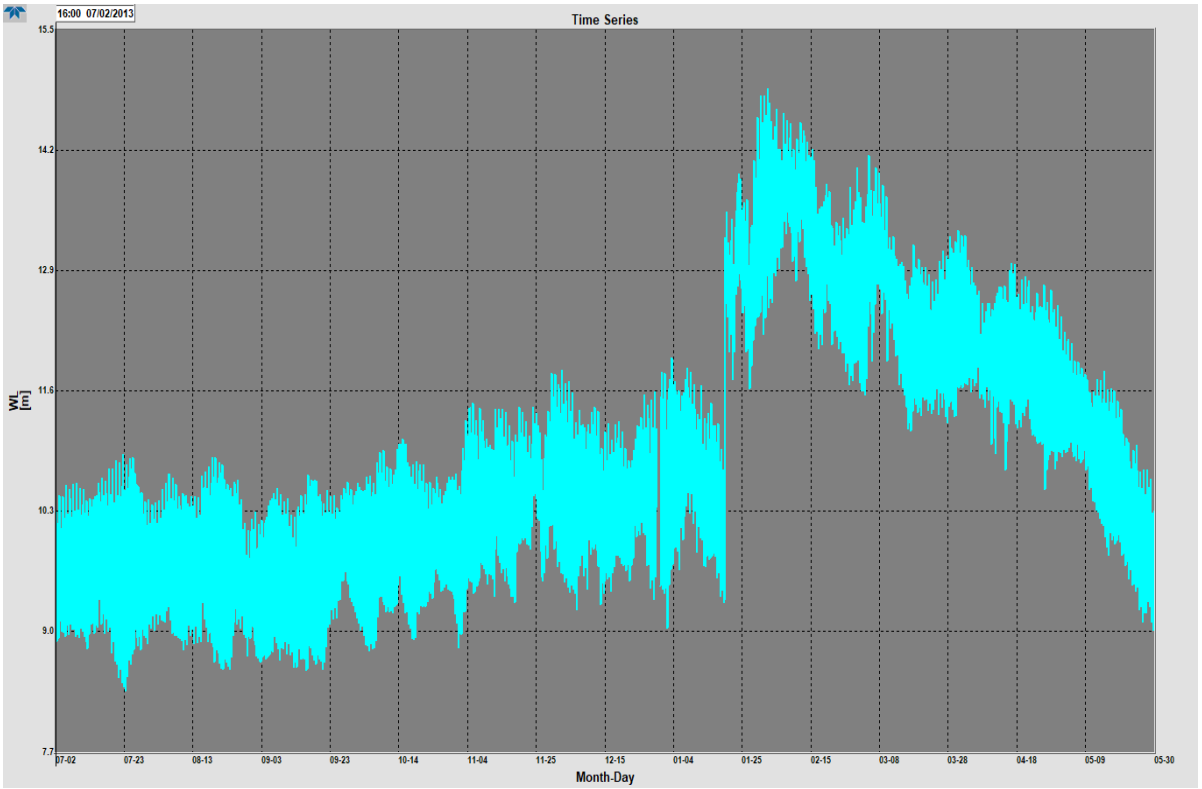

Figure 3-4 WaveView display: Pressure tracking (WL) 'water level/depth'. Pressure transducer malfunction around January 19th, 2014.

Since the display using pressure tracking showed a malfunction in the water level, the data were re-processed using surface tracking to measure the water level – see Figure 3-5. This configuration returned data that were more in-line with expected values. All data were verified with the tide measured data at Fernandina Beach and at the North Jetty, and data were in close agreement with one another. Since the WavesMon configuration for re-processing data is limited to pressure or surface tracking, the decision was to limit any further analysis of the data, to end the wave record on mid December 2013, and to analyze five months of data (July 2013 through December 2013).

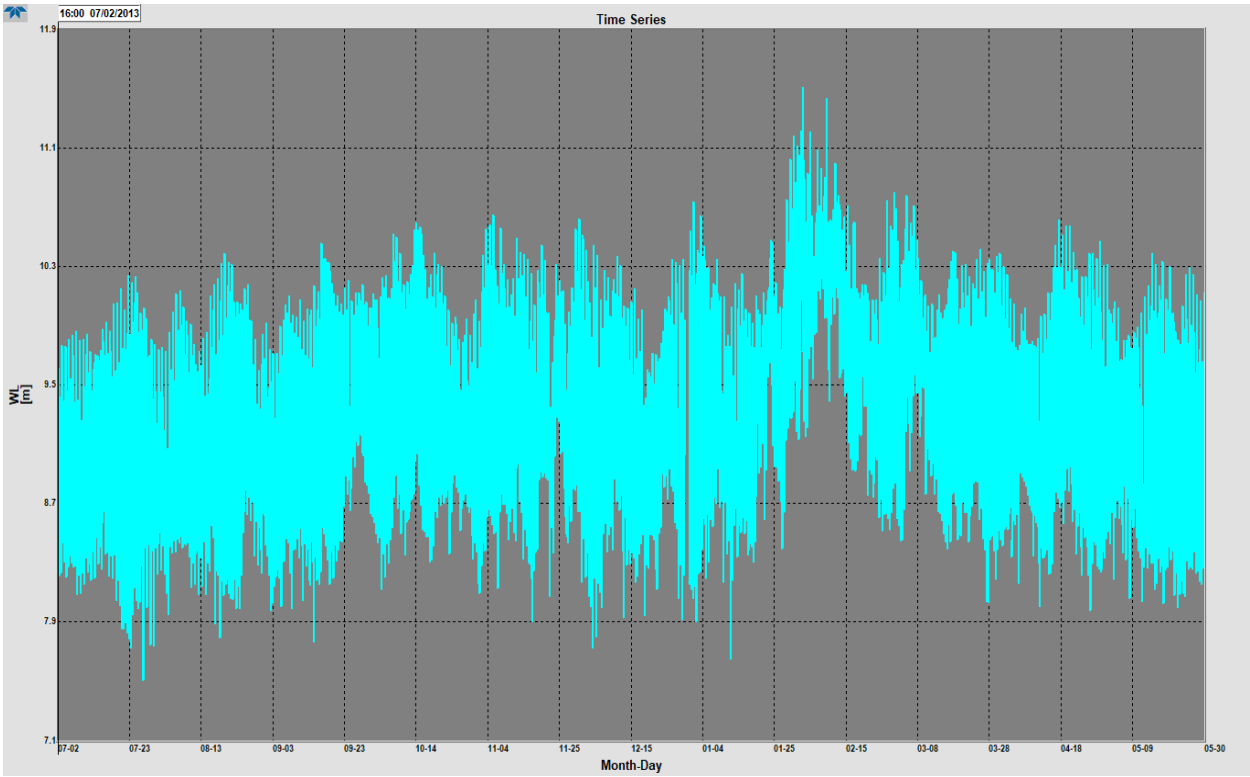

Figure 3-5 WaveView display: Surface tracking (WL) 'water depth'. No malfunction on January 19th, 2014.

To further verify the data, another set of analysis was conducted using the full dataset (i.e., July 2013 through June 2014). The measured were plotted at the tide gauge at Fernandina Beach, and the tide predictions at the North Jetty – see Figure 3-6. In this figure, the instrument elevation was not set at the 1m above the seabed and can be seen in the difference between the surface (blue) and pressure (red) plots below. This issue is addressed in Figure 3-7 to align the pressure and surface tracking configuration by simply setting the instrument elevation at 1m above the seabed.

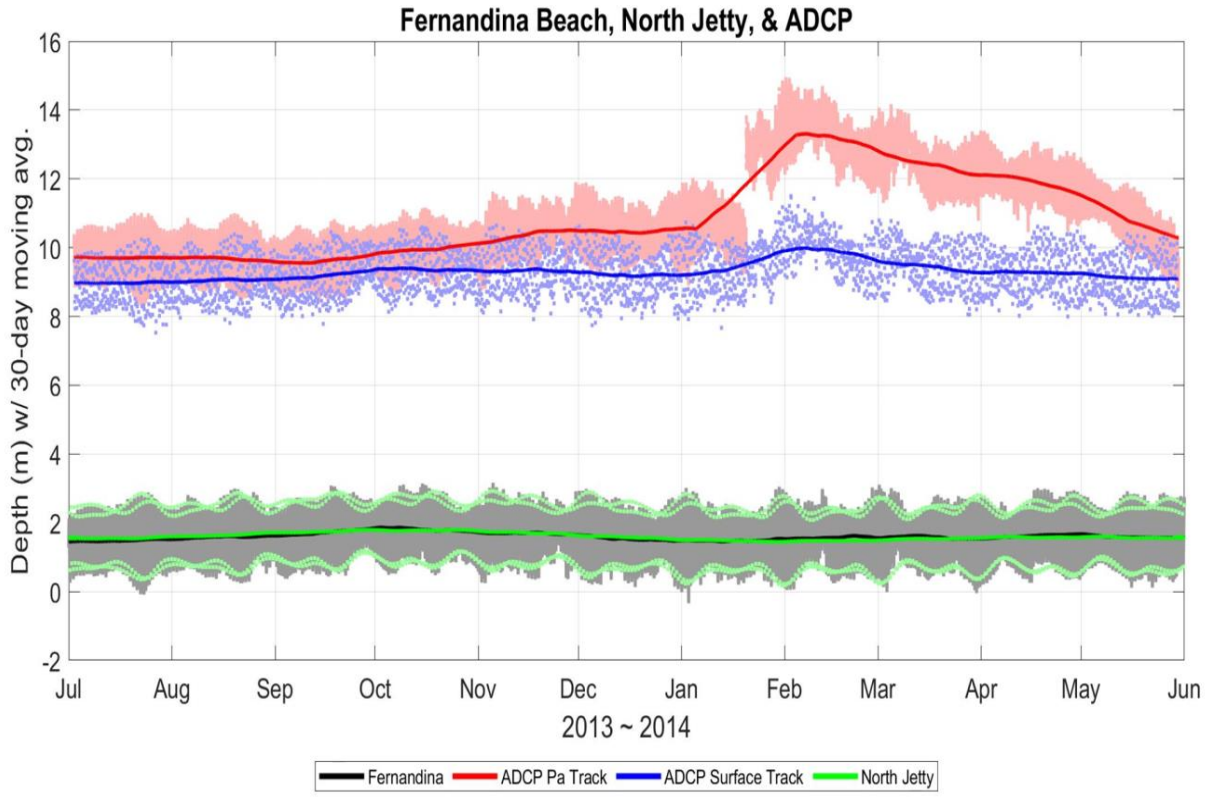

Figure 3-6 Comparison of 30-day moving average of the ADCP data with both configurations of surface tracking (in blue) and pressure tracking (in red), along with the measured tide gauge at Fernandina Beach (in black) and the tide predictions at the North Jetty (in green).

Figure 3-6 shows the anomalous data that began to occur in late 2013 and provides further justification for limiting the dataset through December of that year.

As mentioned above, in Figure 3-7, the pressure and surface tracking configuration were aligned to account for instrument elevation at 1m above the seabed. This figure is a 10-day plot to show that pressure and surface tracking agree and also align with the measured data at the NDBC buoy. The 10-day time series plots measuring significant wave height for both Pressure and Surface tracking, NDBC and ADCP data, and configuration records are illustrated individually in Appendix B.

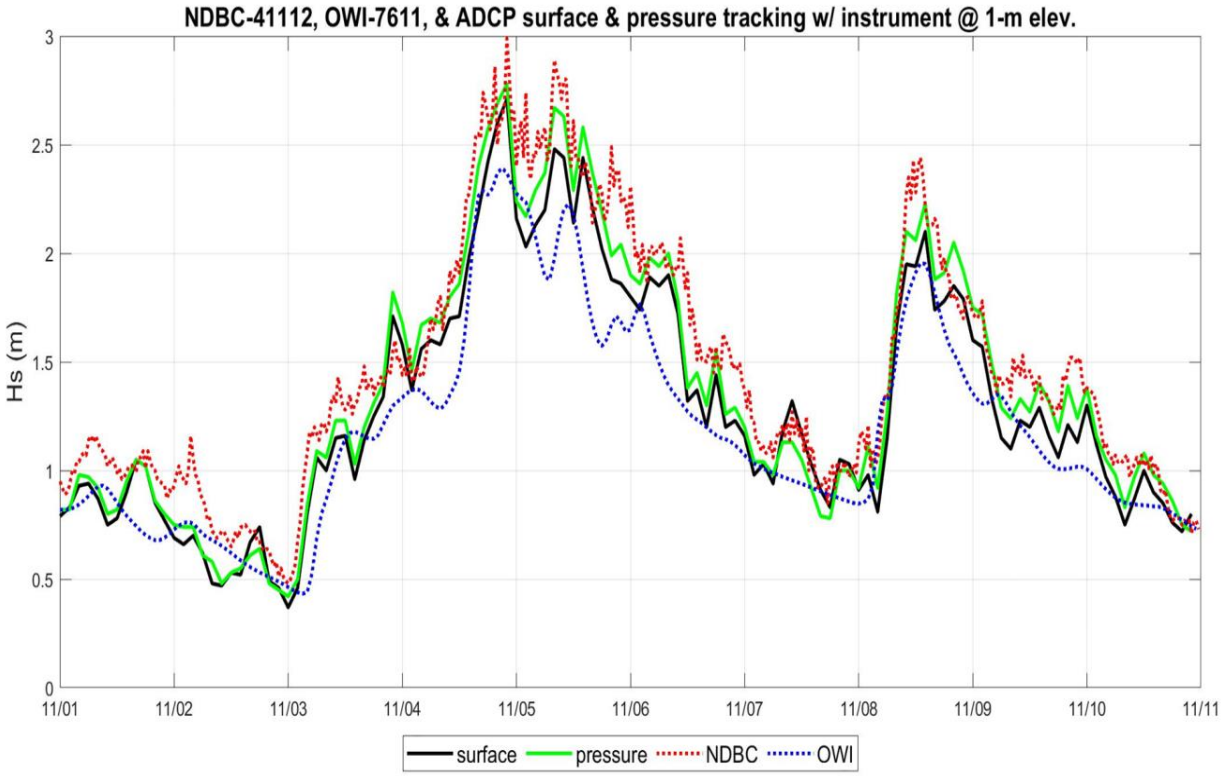

Figure 3-7 Comparison of pressure and surface tracking data with OWI and NDBC data.

CHAPTER 4

Deepwater Hindcast Information

4.1 Why hindcast information?

In the present study, if a suitable wave measuring instrument (*e.g.*, a directional Waverider buoy or an ADCP) had been located well offshore of Mayport in deep water, taking wave measurements concurrent with those taken with the nearshore ADCP, a hindcasted wave record would not be needed to drive the STWAVE+ cross-shelf wave transformation model. Consequently, a deepwater hindcast record was required to utilize as the offshore input to the STWAVE+ model.

"Hindcast" essentially is a methodology through which historical oceanic and atmospheric data/estimates are used to drive a physics-based numerical model for wind-wave generation and propagation *in the past* – hence the moniker "hindcast". Hindcast models have been applied in spatial domains as small as individual lakes and as large are the entire North Atlantic. The main reason for hindcasting wave *information*, which is not real "data" as such, is that records of directly measured wave data are usually of insufficient length to provide a comprehensive wave climate, especially one that includes many extreme storm events. In other words, it is very unlikely that long term data of currents, waves, and winds captured during extreme oceanic events are available to apply, *e.g.*, in a probabilistic model to calculate the design loads on an offshore or coastal structure. Indeed, there are a few sites in which moored buoys or instrumented platforms have collected measured data for more than two or three decades. However, even three decades of continuous measurements may be insufficient to capture the true variability and possible extremes of the wave climate at those sites. Therefore,

even if measured data are available, it is still most prudent for designers and other practitioners to rely on long-term information that is produced through the hindcast approach (Gallagher, Tiron, & Dias, 2014).

4.2 Oceanweather, Inc. Deepwater Hindcast

One of the well-regarded commercial sources of hindcast weather and wave information is Oceanweather, Inc. (OWI). OWI is consulting firm that provides the shipping, petroleum, and ocean/coastal engineering communities with a wide range of services, including hindcasting of environmental information, such as wind, wave, current and surface elevation fields over desired time periods (Woolf & Mcilvenny, 2011). OWI specializes in developing highly refined time series of the wind fields during storm events, for use in driving a wave hindcast model, OWI3G, which is very similar to the well-known model "WAM" (oceanweather, 2006). OWI has produced very-long-term hindcasts, e.g., 1954-2018, for the entire North Atlantic, known as GROW Fine North Atlantic Basin (oceanweather, 2006), but on a relatively coarse numerical grid with a resolution of 30-minute spacing (0.5 degrees latitude by 0.5 degrees longitude).

The situation described in Section 4.1 applies to the present study, for which direct wave measurements in deep water are not available, and so the use of a hindcast record is necessary. More recently, OWI has offered a product similar to GROWFAB, but on a much finer grid (0.05^o x 0.05^o, or roughly 5.6 km x 5.6 km) nested within the coarse-grid global hindcast. The high resolution third-generation spectral wave model, OWI3G, was again employed by OWI to conduct this hindcast, known as GROW-FINE U.S. East Coast (GF-EC). As shown in Figure 4-1, the finer grid stretches from latitude 25.00^o N to 45.85^o N, and from longitude 82.00^o W to 64.3^oW, comprising 29,994 active points. This finer grid system has enabled the domain of the

hindcast model to extend closer to the coasts, where in some locations bottom friction becomes important and for which a bottom friction algorithm is now included in the OWI3G model.

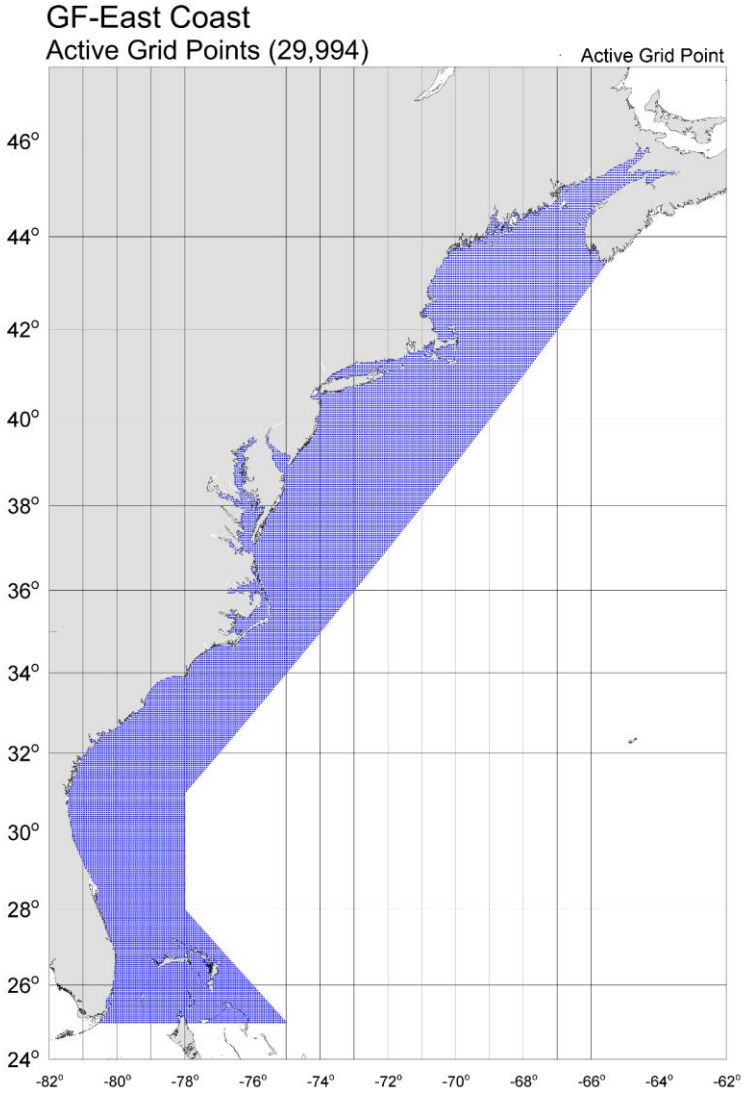

Figure 4-1. The domain and associated grid of the GF-EC project (oceanweather, 2022)

In developing GF-EC, OWI used the General Bathymetric Chart of the Oceans (GEBCO2014) database to model the bathymetry throughout the domain, which is referenced to mean sea level. The GF-EC bathymetry with depths from 0-500m is depicted in Figure 4-2.

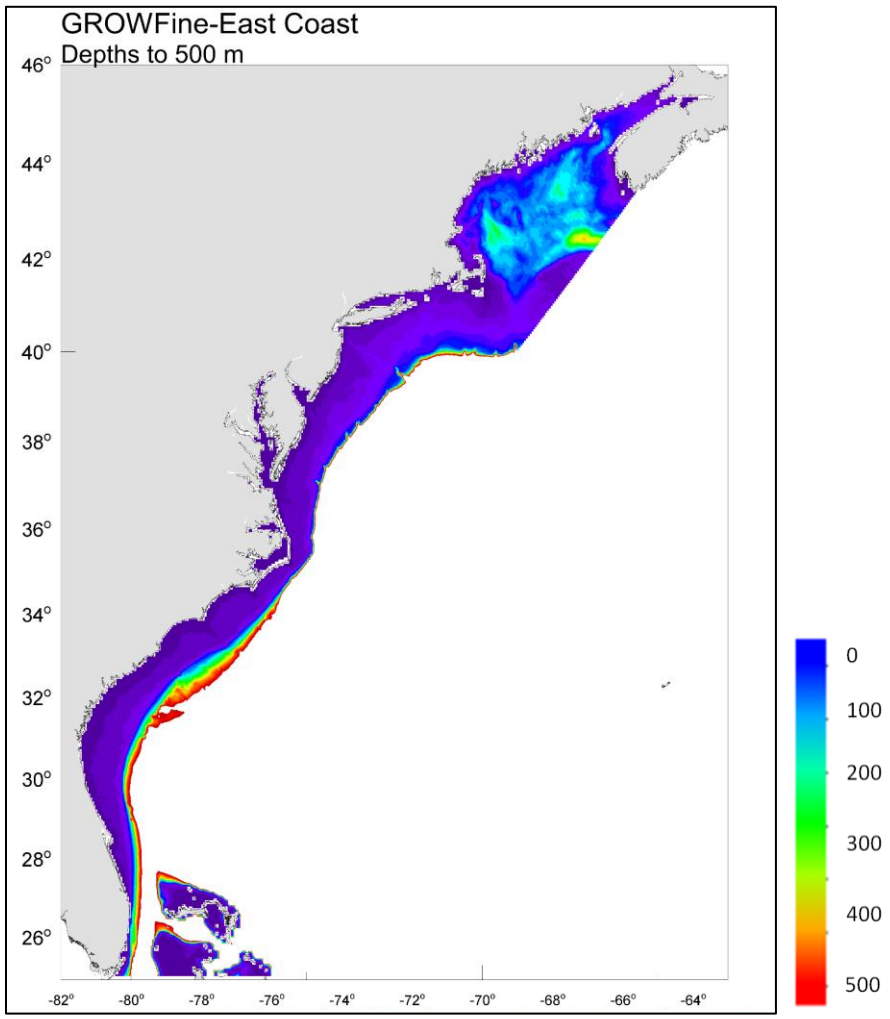

Figure 4-2 - Water depths (0-500 m), referenced to mean sea level, in the domain of the GF-EC hindcast wave model (oceanweather, 2022)

At the grid nodes selected for archiving, the GF-EC product contains a variety of oceanographic data, including the time series of local winds, frequency-direction wave spectra, reported in 26 frequency bins and 48 direction (7.5-degree) bins. Spectral parameters are also available, including, *e.g.*, significant wave height (H_s), peak wave period (T_p), and peak wave direction (D_p), statistical analysis of the output, and results from specific of tropical and extratropical storms. The locations and local water depths at each of the five archived nodes

utilized herein, as well as that for the ADCP and NDBC-41112, are provided in Table 4-1. These locations, in relation to the boundary of the STWAVE+ grid adopted for the modelling effort described in Chapter 5, are shown in Figure 4-3.

Table 4-1 – Location in latitude & longitude and Florida State Plane coordinates, distance from the shore, and the local mean water depth for each of the OWI hindcast nodes, the NDBC buoy, and the ADCP.

Node/Instrument	Latitude, Longitude (WGS84)	Easting, Northing (NAD83)	Distance offshore (km)	Depth (m)
OWI-7611	30.70°N, 81.30°W	705502, 171261	12	12.8
OWI-7198	30.40°N, 81.25°W	672234, 175977	14	14.5
OWI-7130	30.35°N, 81.25°W	666691, 175965	14	16.0
OWI-7062	30.30°N, 81.25°W	661149, 175953	14	16.5
OWI-7203	30.40°N, 81.00°W	672207, 199700	38	24.5
NDBC-41112	30.71°N, 81.29°W	706609, 172222	13	16.0
ADCP	30.37°N, 81.37°W	668940, 164435	3	9.5

Although hindcast nodes 7198 and 7130 are closest to the nearshore ADCP and potentially could be used to drive the STWAVE+ model, a comparison of the hindcast results at 7611 to the nearby wave buoy 41112, described in detail in Section 4.3 below, clearly indicate that the hindcast results at these inner nodes are unreliable. Consequently, in the present study the OWI results archived at 7203, *i.e.* the node located furthest offshore (38 km) and in the deepest water (24.5 m), was used as the input for running the STWAVE+ wave transformation model.

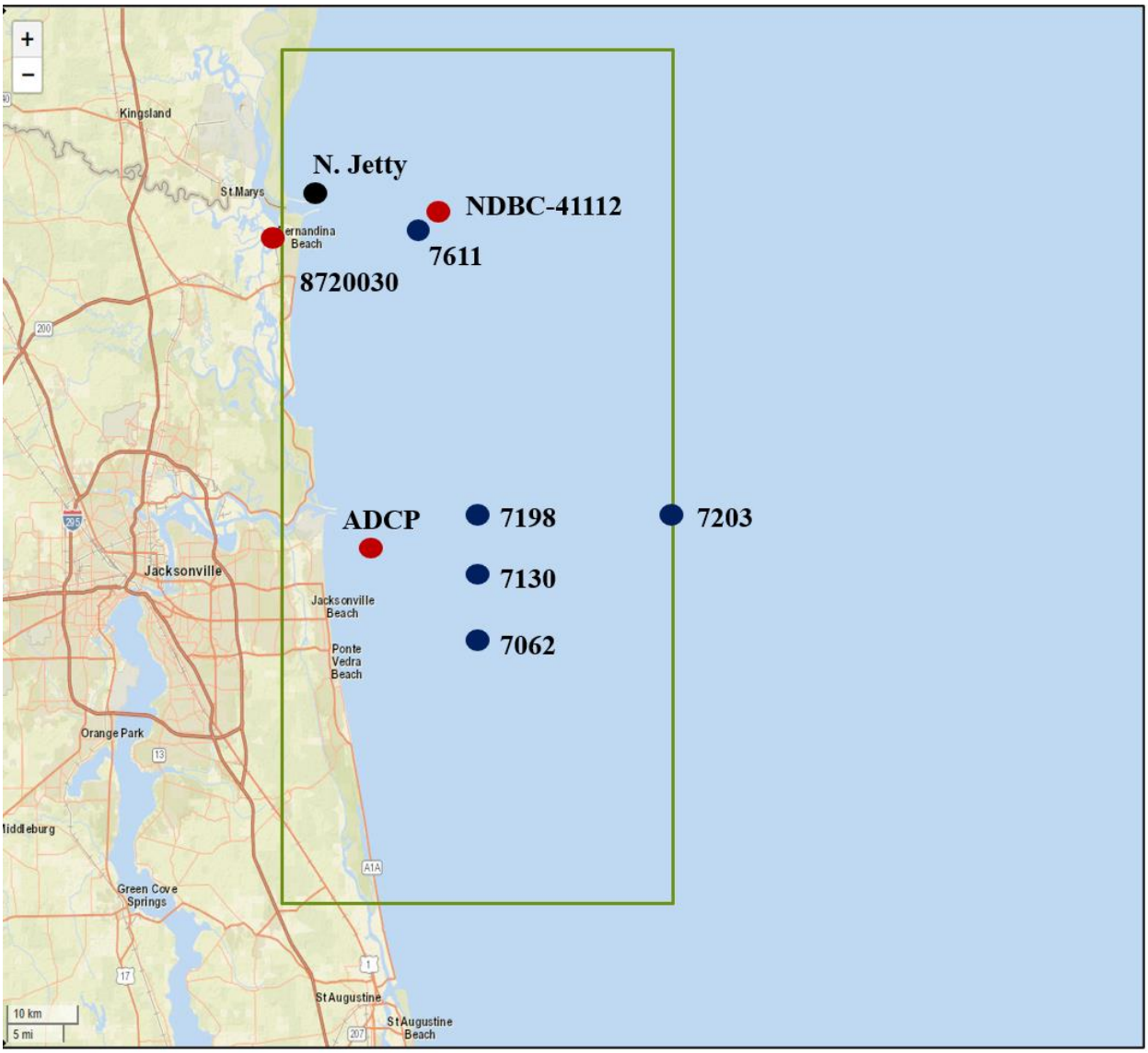

Figure 4-3 – Locations of archived hindcast results and astronomic tide predictions (black dots), wave and water level measurements (red dots), and the boundary adopted for the STWAVE+ modeling.

4.3 Comparison of OWI-7611 Hindcast Results to NDBC-41112.

Because of their proximity and time-concurrent records, direct comparison of the OWI hindcast results at OWI-7611 to the nearby directional Waverider buoy, NDBC-41112, is an extremely valuable exercise in testing the veracity of the GF-EC results at a most-nearshore,

shallow-water node. The spectral wave parameters that are to be compared are a spectrally derived wave height, wave period, and wave direction. The comparison is conducted for the same ~11 months that the ADCP was deployed, i.e., July 1st, 2013, through May 31st, 2014.

In Table 4-2, nomenclature is provided for each of the parameters to be compared. Firstly, the energy-based significant wave height (H_s and H_{sig}) is defined for both the ADCP data (H_s) and the OWI hindcast (H_{sig}) as ; $H_{sig} = 4\sqrt{m_o}$, in which m_o is the total energy contained in the frequency-direction spectrum. Because this is a parameter that is determined by integration, it is usually very stable, changing gradually over time. Peak period (T_p) is defined as the reciprocal of frequency for the bin in the frequency spectrum that contains the most energy density. When, *e.g.,* the locally generated, high frequency sea, and any low frequency swell propagating from a far-away storm each contain equivalent amounts of energy, this parameter can become very unstable, switching back-and-forth between short-period and long-period values. Finally, the ADCP reports the peak direction (D_p) as the bin in the direction spectrum (*i.e.* integrated across all frequencies) that contains the most energy density, whereas OWI defines a "dominant direction" (DomDr) as the maximum of a parabola that has been fitted through the bin containing the most energy density and its two adjacent bins. Once again, at times when wave fields from two distinct directions contain equivalent amounts of energy, these parameters can become unstable, switching between two highly different directions.

Table 4-2 Nomenclature for spectral parameters derived from the specific data.

Name	NDBC	OWI
Significant Wave Height (m)	H_s	H_{sig}
Peak Wave Period (sec)	T_p	T_p
Peak Wave Direction (deg)	D_p	DomDr

It is important to note that for the NDBC measurements "direction" is regarded as the direction *from which* waves approach (degrees clockwise from True North), whereas the OWI directions are reported as direction *to which* the waves are propagating. Consequently, 180° is added to the NDBC directional values (and if the result is greater than 360^{o}, 360 is then subtracted) to render them consistent with the OWI convention.

Figure 4-4 presents a comparison of the time series for the three wave parameters as hindcasted at OWI-7611 and measured at NDBC-41112 for the month of October, 2013 (H_s, T_p, D_p/DomDr). It is seen that both hindcast and measurements of H_s are smooth and well-behaved, although the hindcast appears to underpredict the measurements, particularly during the two storm events. In the middle panel, the measurements of T_p at the buoy indeed display momentary switching from the predominant long-period waves to short-period waves, during which the hindcast consistently seems to be "fooled" into choosing the shorter period sea, *e.g.* from the 3^{rd} - 5^{th} and from the 10^{th} – 14^{th}. In the bottom panel of Figure 4-4, the measured peak wave directions are generally well-behaved, only suddenly switching directions on the 5^{th}, 14^{th}, 20^{th}, 23^{rd}, and 25^{th}; however, the hindcast seems to do well in representing these shifts. The time series plots for the wave parameters for each month in the record are provided individually in Appendix A.

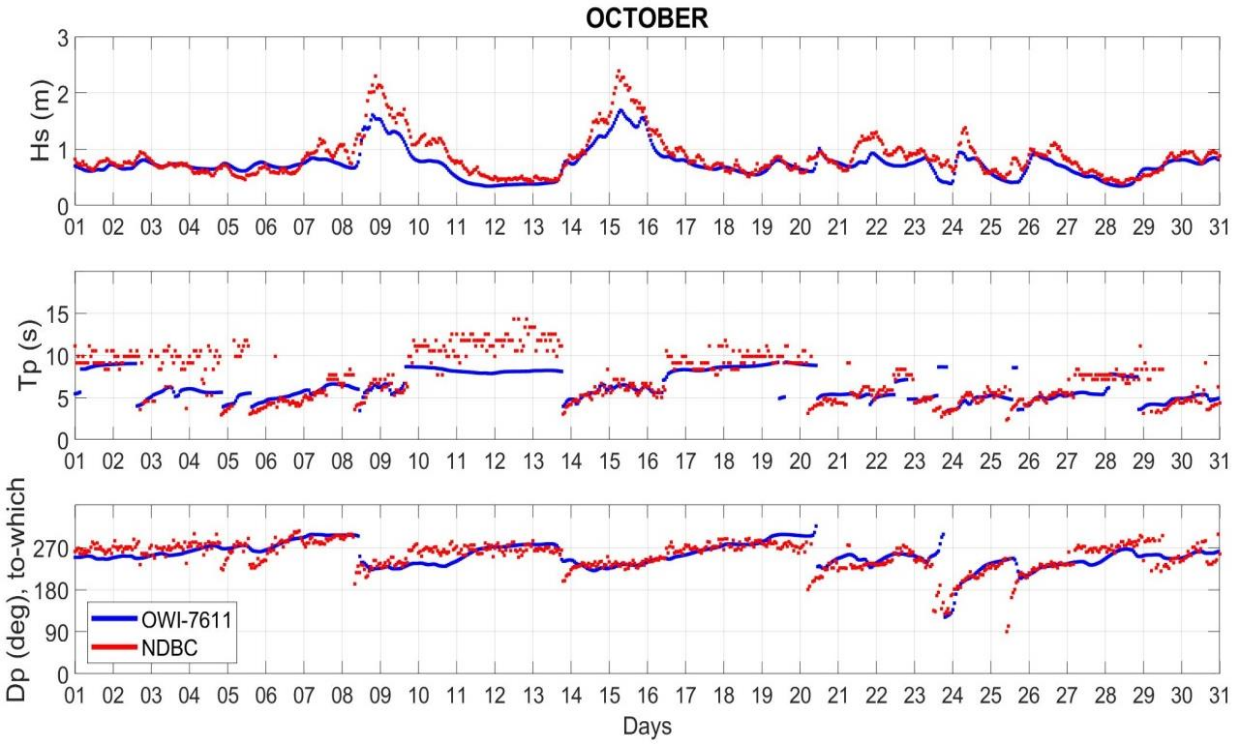

Figure 4-4 Time-series comparison of wave parameters from the hindcast at OWI-7611 to the measurements at NDBC-41112.

Figure 4-5 presents the time series of H_s from both NDBC-41112 and OWI-7611 covering the entire eleven-month span from July 1st, 2013, through May 31st, 2014. The red line is the measured NDBC data, and the blue dots are the OWI hindcast results. It is apparent that the hindcasted heights consistently underpredict the NDBC measurements, particularly during storm events. This is also apparent in detail in the monthly plots provided in Appendix A.

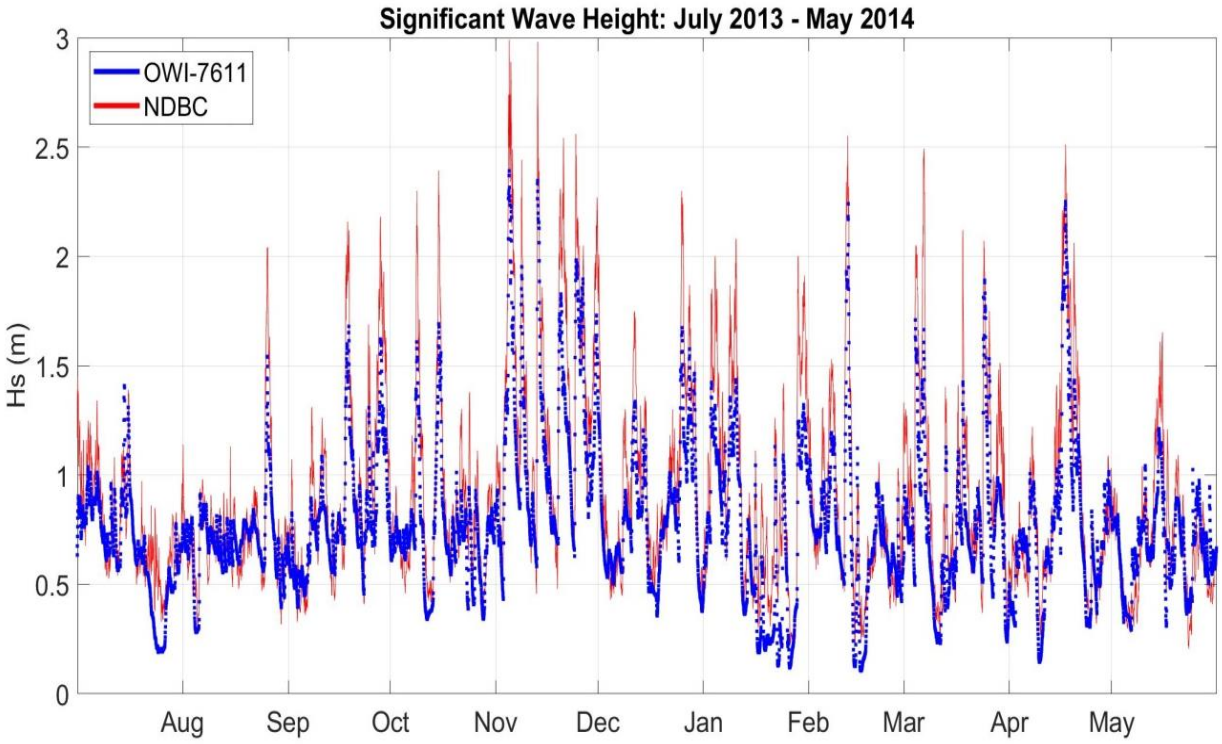

Figure 4-5 Time series of OWI results versus NDBC measurements of significant wave height (Hs) during the entire eleven months the nearshore ADCP was deployed.

Figure 4-6 presents a scatter plot for H_s from the OWI-7611 hindcast as compared to the NDBC-41112 measurements, and again confirm that the OWI results underpredict H_s at this location.

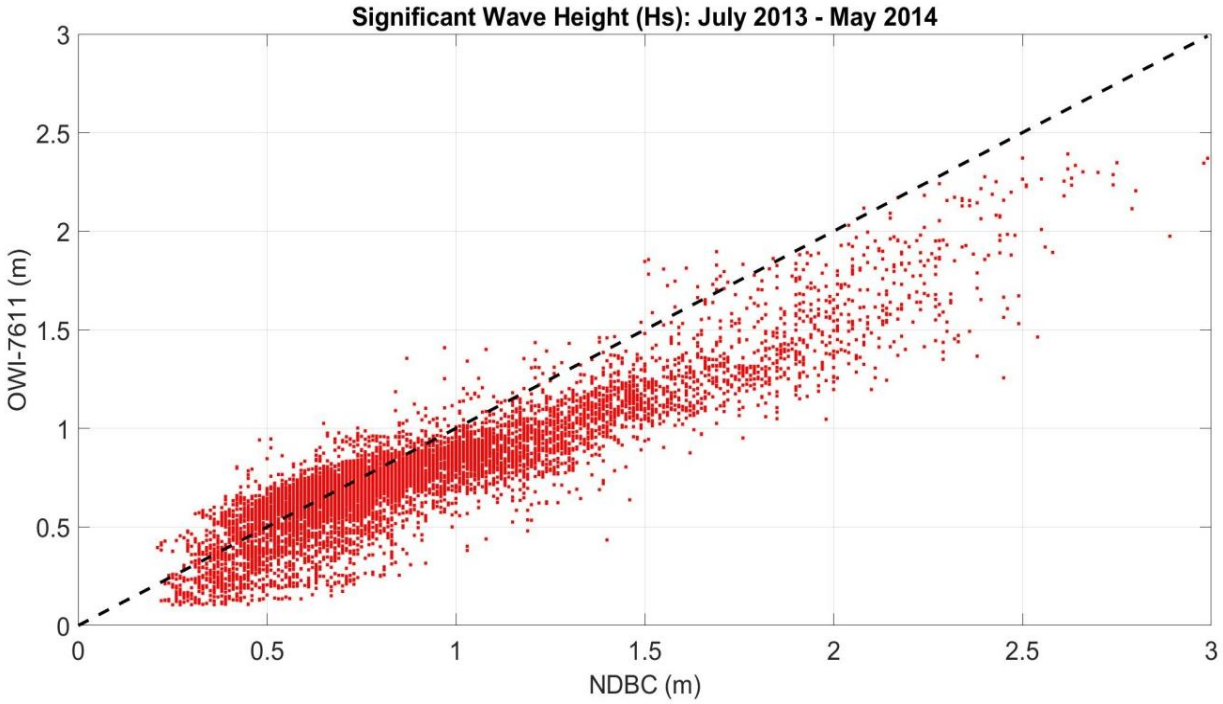

Figure 4-6 Scatter plot of significant wave height (Hs) for OWI-7611 vs NDBC-41112, for the entire eleven-month record.

Based on the figure above, the scatter plot may not tell us the whole story, so we attempt to use further statistical analysis in the form of a quantile-quantile (Q-Q) plot. The concept behind a Q-Q plot is to see if the quantiles of the first data set match with the quantiles of the second data set. If all the point quantiles are the same or close to a straight line, then they have similar distribution, otherwise they will have a dissimilar distribution. The Q-Q plot will be shown later in Chapter 7 when comparing the different friction coefficients (C_f).

Based upon Figure 4-4, Figure 4-5, and Figure 4-6, it is clearly demonstrated that for the eleven months of record, the hindcast results at OWI-7611 significantly underpredict the nearby buoy measurements, especially during storm events.

CHAPTER 5

Description of STWAVE+

5.1 STWAVE+ Spectral Wave Model.

The original STWAVE (STeady-state spectral WAVES) introduced by Smith, Sherlock, and Resio (2001) is a "second-generation" model for wind-wave generation, propagation, and transformation due to basic wave processes. In deepwater it simulates wind-wave growth, nonlinear wave-wave interactions, and white-capping, which redistribute energy in both frequency and direction and dissipate energy in a growing wave field. In transitional water, the model simulates depth-induced wave refraction and shoaling, current-induced refraction and shoaling, and steepness-induced wave breaking, In very shallow water, depth-limited breaking is induced. STWAVE does not rigorously simulate wave diffraction, particularly at coastal structures, as is a common misconception of users. It is referred to as a "second-generation" (2G) wave model because it uses a parameterization to represent nonlinear wave-wave interactions, whereas "third-generation" (3G) models such as OWI3G attempt to rigorously compute these interactions and the resulting redistribution of wave energy. However, 1) there remains an ongoing disagreement among wave modelers as to the correctness of the interaction methods used by the 3G models, and 2) the numerical integration required by the 3G models greatly increases CPU requirements.

As with all present-day spectral wave generation models, STWAVE is based on the assumption that phase information is not tracked, *i.e.*, it is a phase-averaging model because the relative phases of the spectral components are assumed to be random. Other assumptions are:

Mild bottom slope and negligible wave reflection. The original version of STWAVE is a halfplane model, so wave energy can transfer only from the offshore toward the nearshore (±87.5 deg from the x-axis of the grid). Waves reflected from the shoreline, from steep bottom features, or are otherwise outside the directions within the half-plane are not represented by the model. STWAVE has since been cast as a full-plane model (Smith et al., 2001); however this has increased the CPU requirements by an order of magnitude.

*Spatially homogeneous offshore wave c*onditi*ons.* The input wave spectrum along the offshore boundary of a model domain is assumed to be uniform. Yet, for domains with a longshore dimension less than 100 km, this variation is usually negligible (Smith et al., 2001).

Steady-state waves, currents, and winds. In STWAVE the wave growth is assumed to have reached a steady-state, which implicitly assumes the wind speed and direction remained sufficiently steady for the waves to have attained a fetch-limited or even fully developed state.

Linear refraction and shoaling. Because STWAVE utilizes linear wave theory to determine refraction and shoaling, it is not able to model the effects of nonlinearity of waves as they enter shallow water. Especially for large Ursell numbers ($U = H\,L^2/h^3$) a nonlinear wave has a shorter yet higher crest elevation and a longer but reduced trough than a sinusoidal (linear) wave containing the same mean energy. This results in an increase in wave celerity and group velocity, thereby affecting the refraction and shoaling processes.

Negligible wave energy losses due to bottom friction. The earlier versions of STWAVE (*e.g.* 3.3) neglected the energy losses attributed to bottom friction, which is now well-recognized to be

important as waves pass into intermediate water depths and especially as they enter shallow water.

5.2 Incorporation of Bed Friction: "STWAVE+"

William R. Dally and Osiecki (2004) addressed the bottom friction issue in early versions of STWAVE, and added a simple subroutine to STWAVE v3.3 to explicitly account for these losses, based upon the following representation.

Wave energy losses due to bottom friction are based on the assumption of a turbulent boundary layer at the sea bottom (Nielsen, 1992), for which one of the most conventional formulas for bed shear stress is:

$$\tau_b = \rho C_f u_b |u_b| \qquad (2)$$

in which ρ, C_F and u_b denote water mass density, a dimensionless drag coefficient and the fluid velocity near the bed, respectively. The phase-averaged rate of energy dissipation, ε_F,assuming harmonic flow, for a unit area over a wave period, T, is:

$$\varepsilon_F = \frac{1}{T}\int_0^T \rho C_f {u_b}^2 |u_b| dt \qquad (3)$$

Applying linear wave theory to provide the near-bed fluid velocity in the above equation yields:

$$\varepsilon_F = \frac{\rho C_f \frac{4}{3}\pi^2 f^3 H^3}{sinh^3 kh} \qquad (4)$$

in which f, H, k and h represent wave frequency, wave height, wave number and water depth, respectively. This is a common means of estimating the rate of energy dissipation due to bed friction (see Dean and Dalrymple (1991)), but usually requires *in situ* measurements to establish a reliable value for C_f, which can vary over two orders of magnitude depending on the bed roughness and composition, as indicated in Table 5-1.

Table 5-1 Range in friction factor (C_f), applicable for the bed stress model defined by Eq. 2, for various types of bed compositions.

Bed Composition	Friction Factor Range (Typical)	Reference
Flat sand	0.0025 – 0.05 (0.005)	Kamphuis, 1975
Rippled sand	0.003 – 0.25 (0.10)	Nielsen, 1992
Reef	0.05 – 0.25 (0.15)	Gerritsen, 1980

5.3 STWAVE+ Modeling Structure and Procedure

Figure 5-1 presents the general structure of STWAVE+, with the required input files listed on the left and the list of optional, user-selected output files on the right. For the present study, the only output required were the fields of wave, height, period, and direction.

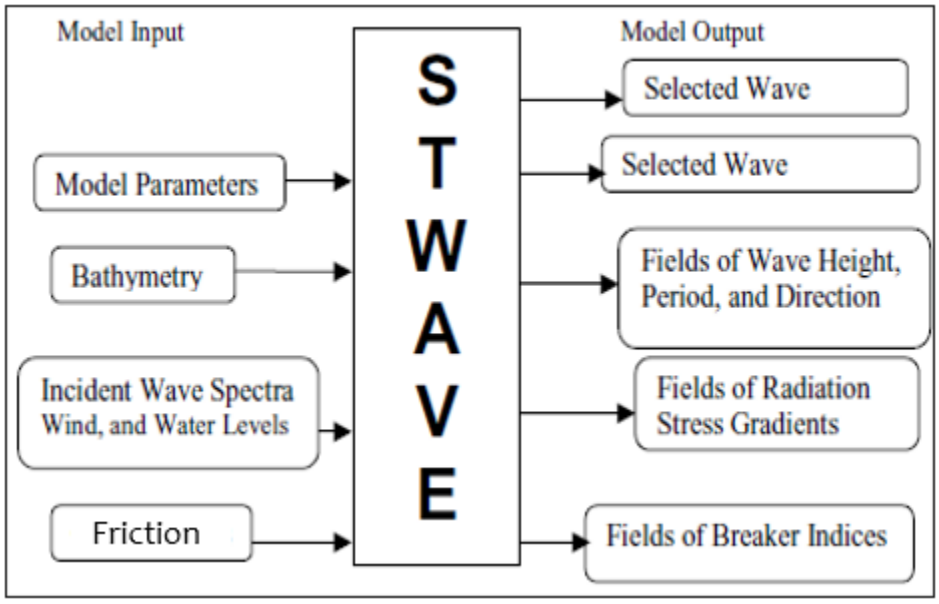

Figure 5-1 STWAVE input and output files (Massey, Anderson, Smith, Gomez, & Jones, 2011).

5.3.1 Spectrum input (spec.in)

It Section 4-3 it was concluded that energy losses due to bed friction were poorly predicted at the nearshore nodes of the OWI grid. This is likely because of the bed friction model utilized in OWI3G (which differs from that derived in Section 5-2) and the fact that the default value for the friction coefficient (based upon the JONSWAP experiment conducted in the North Sea) was adopted instead of being determined by field measurements. Consequently, the offshore node, OWI-7203, was used to provide the input spectra. Firstly, the OWI time series of input spectral frequency-direction files were subjected to interpolation in direction, and then converted into the input format required by STWAVE+. Whereas the OWI spectrum uses a bearing datum of 0° North with the clockwise direction positive, STWAVE+ adopts a right-handed coordinate system, with the x-axis as the bearing datum and counter-clockwise as positive. The cartesian grid is usually constructed with the x-direction pointed onshore. Because it is assumed that the spectrum input file is the only input that changes with each time step (hourly in this case), a batch file of input spectra was created for running the model for the desired length of time.

5.3.2 Bathymetry input (dep.in)

The procedure followed to generate the bathymetric grid required by the model is described in detail in the next chapter. STWAVE+ reads in bathymetric depths as positive values and topographic elevations as negative values. The size of the grid generated is approximately 100 km in the longshore direction and 50 km in the cross-shore direction, with square grid cells of 100 m size.

5.3.3 Bottom friction input (friction.in)

The computation of bottom friction requires an array of assigned friction coefficients, one for each cell in the grid. This array is formatted in the same manner as the bathymetric grid.

5.3.4 Options input (options.in)

The options input file defines the model parameters and specifies the grid cell locations for outputting data. The model parameters are set by a series of five integer-switches contained in the first line of the file. These switches are defined in order as: propagation, wave-current interaction, breaking file output, radiation stress gradient output, and the number of output location points. The first four switches work as 1 (set to on) or 0 (set to off), and the last one can be set to any number within the grid for output location points. Once the output location points are listed, the following lines in the file are the cell spacing locations for the output points.

CHAPTER 6

STWAVE+ Grid Generation

6.1 STWAVE+ Grid Boundaries and Bathymetry Generation

STWAVE is coded and formulated in a staggered grid and the variables are defined using a finite-difference method. Although the mesh cells ought to be square (DX = DY) for half-plane simulations, DX and DY can be different for full-plane simulations. In STWAVE, a local coordinate system is defined, in which the x-axis oriented in the cross-shore direction and the y-axis oriented alongshore, creating a right-handed coordinate system. The grid and the local coordinate are exemplified in Figure 6-1 (Massey et al., 2011).

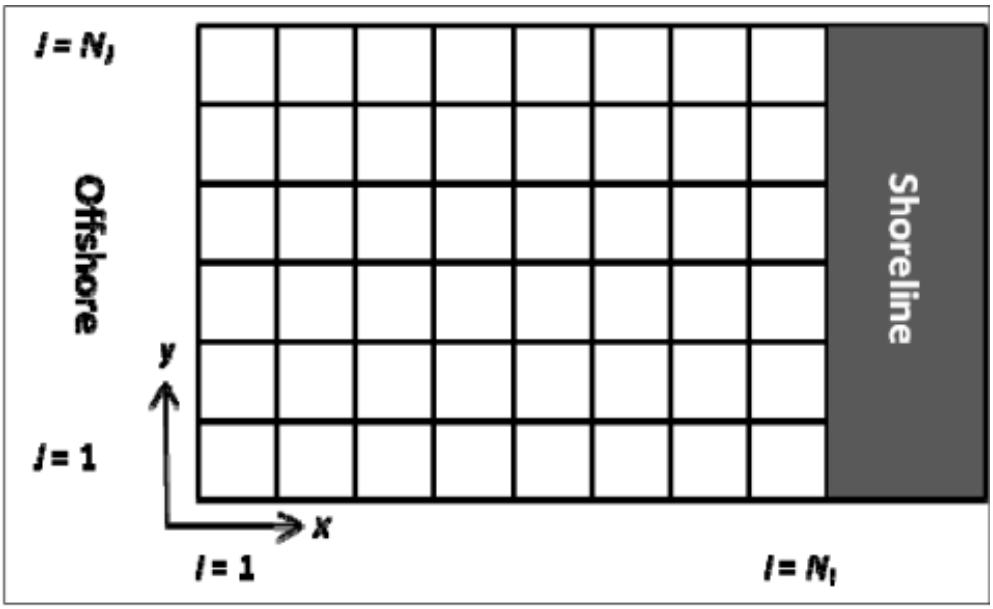

Figure 6-1 Staggered mesh in STWAVE with the local coordinate (Massey et al., 2011)

Typically, the rectangular grid is rotated so that the offshore boundary is roughly parallel with the shoreline. Positive wave angles are defined as counterclockwise from the x-axis.

Lateral boundaries can represent land or water by attributing the required sign - positive denotes water and negative denotes land.

6.2 Global Multi-Resolution Topography (GMRT)

The NSF-supported Marine Geoscience Data System in partnership with the National Geophysical Data Center has produced the Global Multi-Resolution Topography (GMRT) synthesis, a continuously updated digital elevation model that is accessible through the Open Geospatial Consortium. The GMRT Synthesis is a multi-resolution digital elevation model (DEM) managed in three projections and provides an infrastructure for accessing DEMs in the form of grids, images, points, and profiles within a scalable global architecture (Ryan et al., 2009). GMRT consists of ten spatial resolution levels corresponding to 9x magnification (Figure 6-2).

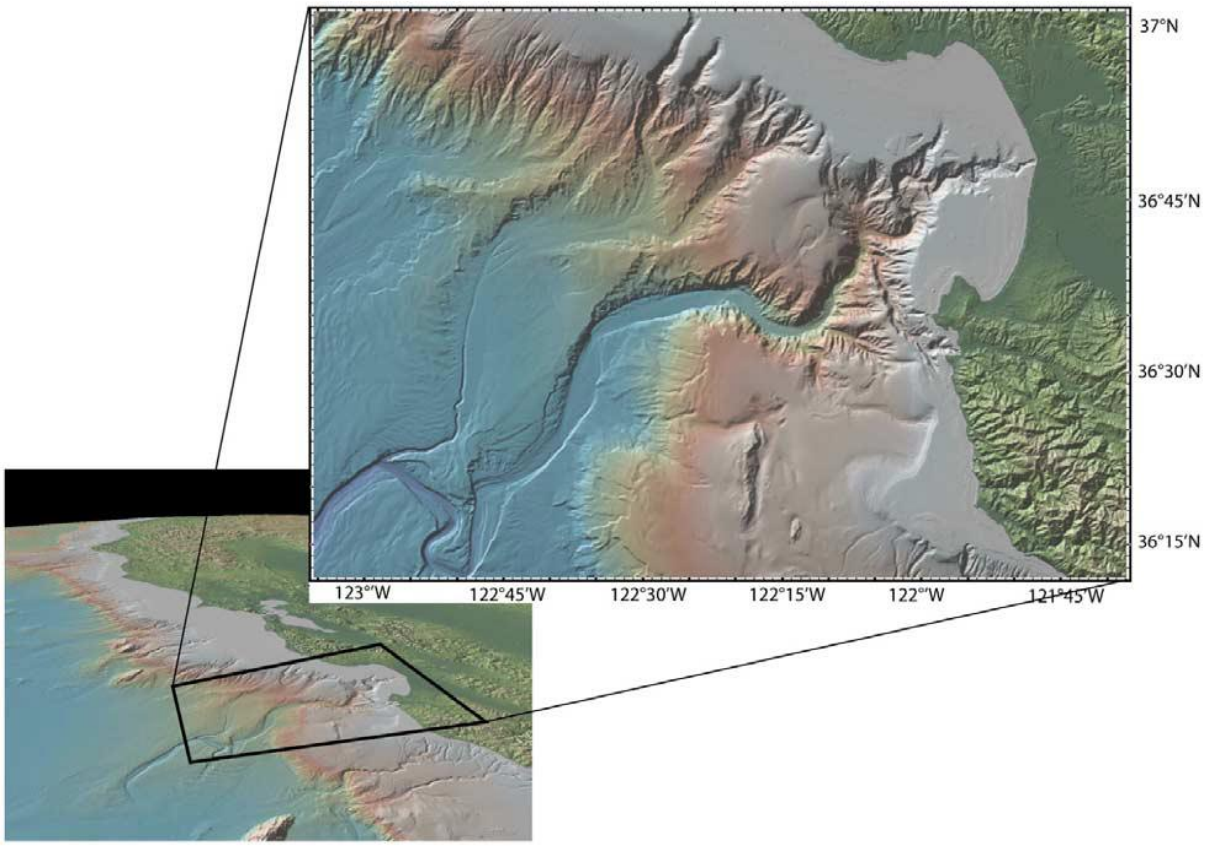

Figure 6-2 Illustration of the multiple resolutions of the GMRT (Ryan et al., 2009)..

The minimum resolution of the GMRT comprises 4 tiles. Enhancing the GMRT resolution by a factor of n is associated with a larger number of tiles by n^2. GMRT contains both the color-shaded relief image and the underlying elevation values at 10 different resolutions up to 100 m. In addition, the GMRT offers four fully complementary tile sets: the gridded elevations in binary format, two imagery tile sets in jpeg format, and a tile set with grid node weights in a floating binary format. GMRT Synthesis provides the marine community with access to bathymetric images and gridded bathymetric data for both professional and non-professional users.

In the present study, after locating the appropriate grid on the GMRT website that encompassed the intended STWAVE+ boundary, three formats were selected to be downloaded so, if any discrepancies occurred, a validated map was still obtainable. The three formats are:

- **grd:** Which is a grid format used to generate maps; contains two-dimensional uniform lattices (regularly spaced, rectangular array) of XYZ data (e.g., easting, northing, and elevation); may be in a binary or text format but is most often saved in the binary format.
- **tif:** A TIF file is an image saved in the Tagged Image File Format (TIFF), a high-quality graphics format. It is often used for storing images with many colors, typically digital photos, and includes support for layers and multiple pages.
- **asc:** An ASCII file is a plain text file that uses ASCII character encoding. You can open and edit an ASCII file in most any text editor or word processor. ASCII files are more commonly saved with the .TXT or .ASC extension.

A screen-shot of the DMRT web-page used to obtain these data is shown in Figure 6-3.

Figure 6-3 Grid download for the aimed location (Ryan et al., 2009)

The grid projection of the saved file conforms to the World Geodetic System 1984 (WGS84), a standard used in cartography, geodesy, and navigation. WGS84 includes a coordinate frame for the Earth, a spherical reference surface (datum or reference ellipsoid) for raw elevation data, and a gravitational equipotential surface (geoid) that defines the nominal sea level. The grid is supplied in latitude/longitude coordinates, and the spacing between grid nodes is 4-arcseconds, which corresponds to a Cartesian length of approximately 122 meters.

6.3 Surfer

STWAVE+ runs on a Cartesian grid with square grids specified in meters. Consequently, it is required to convert WGS84 to a State Plane Coordinate System (SPCS). This is a plane coordinate system only used in the USA, and each state has its own zones according to its size, ranging from 1-6. Using small zones provides a higher level of accuracy. In Florida, the origin for SP83 is located southeast of Key West Florida at approximately WGS84 location: 24°19’14”N, 82°58’13”W. Thus, all coordinates in the SPCS will be in the positive quadrant, with the x-axis denoting easting and the y-axis denoting northing.

The SPCS selected is specific to the location of the study and, in this case, it is NAD 1983 State Plane Florida East FIPS 0901 meters (SP83). To convert WGS84 to SP83, a program called Surfer from Golden Software was used. This program converts irregularly spaced xyz data into an evenly spaced grid, and this output grid can be used to produce a variety of maps, including contour, color relief, and 3D surface (Golden, 2022).

When running the STWAVE+ model, each of the seven grid points of interest listed in Table 4-1; - NDBC-41112, ADCP, OWI-7611, OWI-7198, OWI-7130, OWI-7062, and OWI-7203, was also converted from WGS84 to SP83 using a National Geodetic Survey (NGS) Coordinate Conversion and Transformation Tool (NCAT).

Although Surfer converts the WGS84 grid to a SP83 grid, it does have a few issues. The converted grid tilts slightly, resulting in empty/blank data along the edges. Therefore, it is necessary to edit the grid by cropping out the empty edges while still maintaining a rectangular grid boundary with 100-meter cell spacing. When converting the WGS84 grid to SP83 in 100-meter cell spacing, the Surfer software performs triangulation with linear interpolation to create depth cells at 100-meter intervals. Figure 6-4 is a Surfer dialog box that appears when the SP83

boundary grid is selected and triangulation with linear interpolation is completed for the 100-meter cells in the grid.

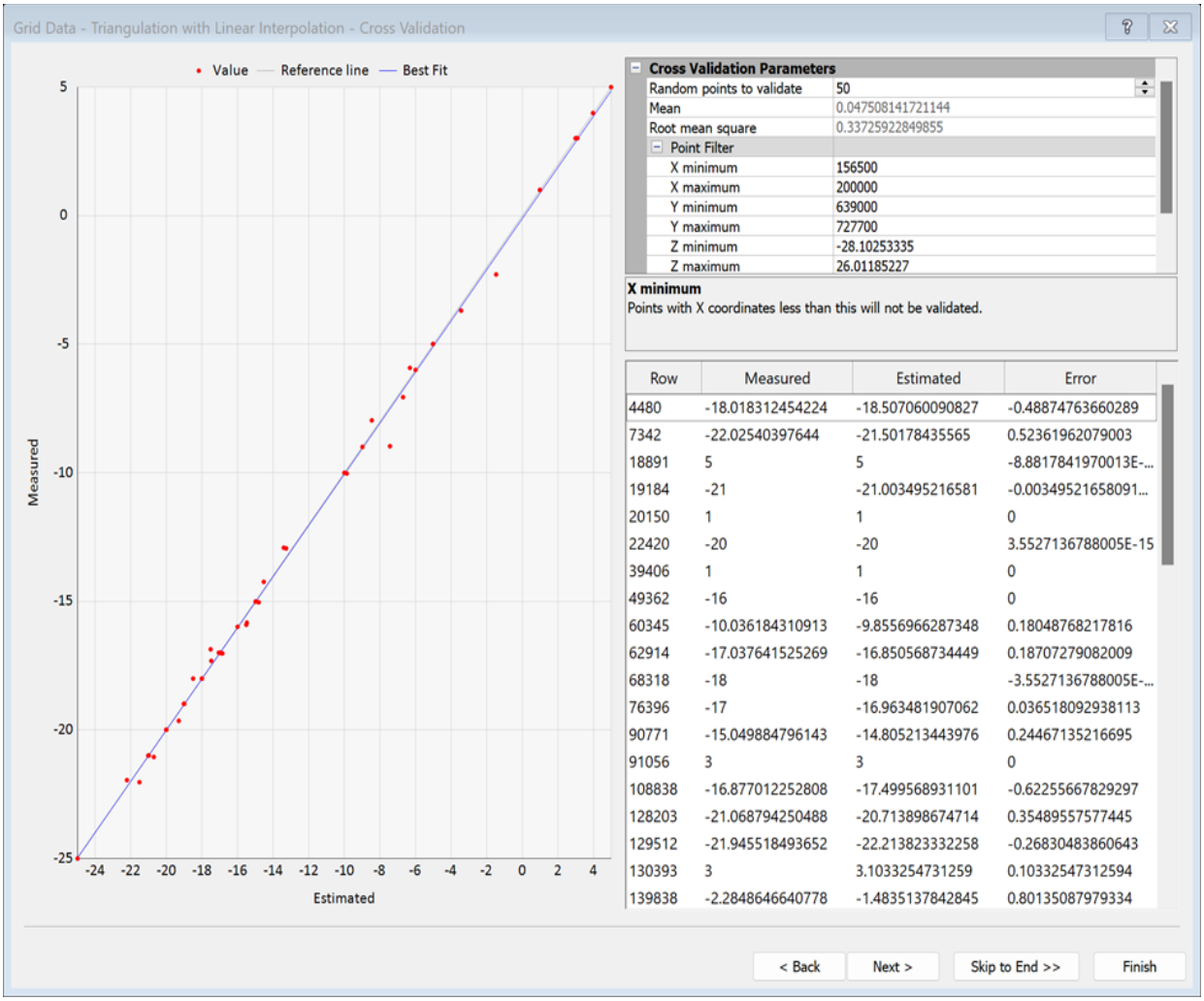

Figure 6-4 Surfer dialog box display showing triangulation and linear interpolation.

The southwest corner of the STWAVE+ grid adopted herein is located at (156800, 639400), and the northeast corner at (199700,727300). The grid is 430×880 cells, with 100-m resolution. A contour/color plot if the bathymetry to be exported to STWAVE+ is shown in Figure 6-5.

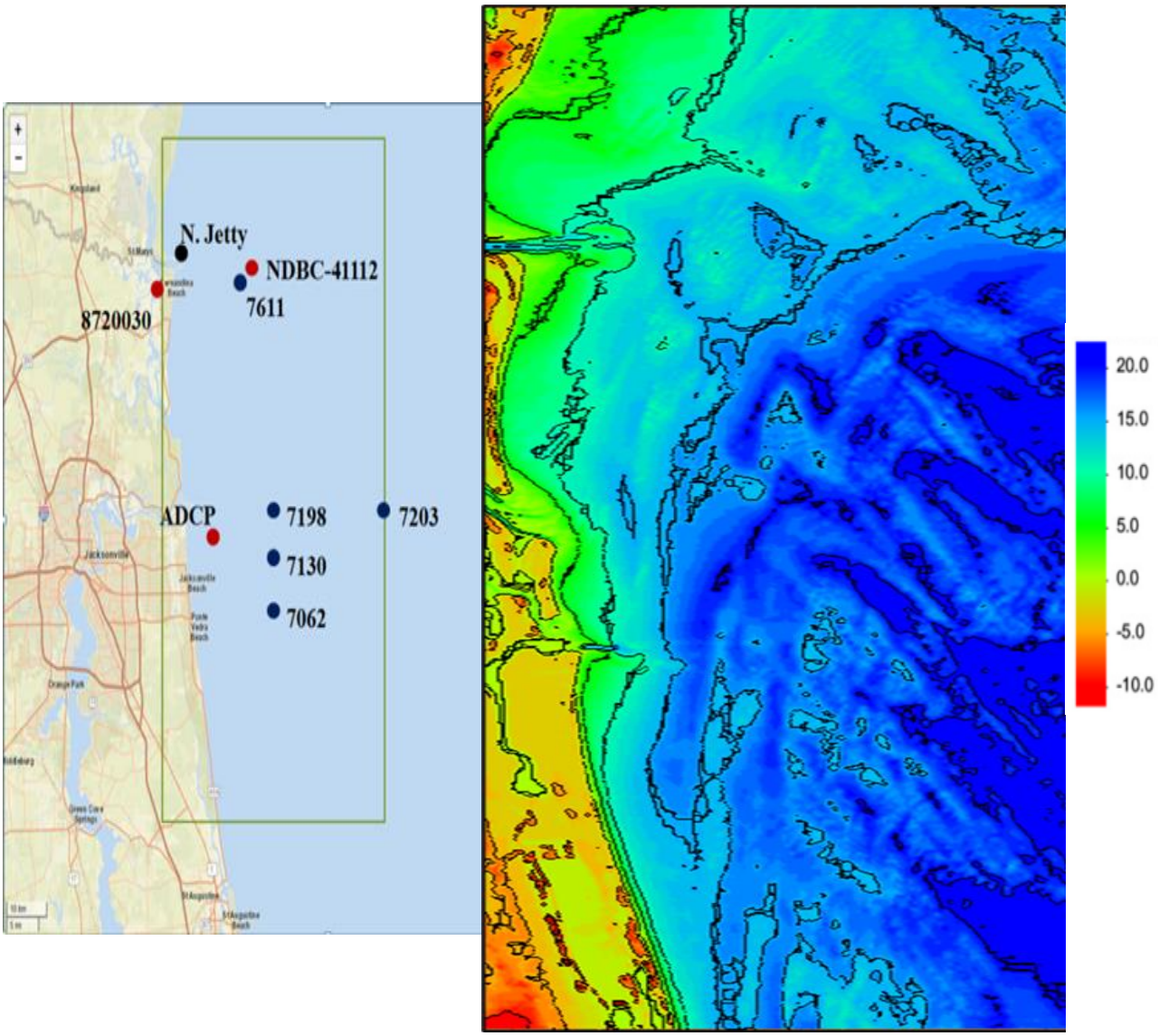

Figure 6-5 Contour and color relief grid exported from Surfer.

CHAPTER 7

Demonstration of the Calibration Methodology and Results

7.1 The Proposed Calibration Methodology

The overall goal of this effort is to propose and demonstrate a general methodology for determining a value for the friction coefficient (C_f) that provides the best estimate of wave energy losses due to bottom friction in the nearshore. A secondary objective is that the methodology be applicable to the many different bottom-friction formulations adopted by the various wave transformation models reported in the literature. The methodology proposed is demonstrated below.

Firstly, with some knowledge of the composition of the bottom, STWAVE+ is run using a realistic range of values for bottom friction coefficients (C_f). Knowing that the sea floor offshore of Mayport is predominantly sandy bed, the values selected are C_f = 0.000 (*i.e.* no friction), 0.010, 0.015, 0.020, and 0.025. Due to computing power limitations (described below) the model was run for only the month of October 2013. Of the eleven months available, this month was selected because 1) it was before the pressure transducer malfunction that occurred in January, and 2) this month contained two significant storm events (see Figure 4-4) during which Hs approached 2.5 m at NDBC-41112.

7.2 Computational Cost (Processing Time)

The STWAVE+ model was performed on an Intel® Core™ i7-9700 CPU at 3.00GHz which contains eight cores. This translated to a 1-hour/time-step of input data for every five minutes of processing time. Due to time constraints, the model was run for 1-month in order select the best candidate friction coefficient (Cf) to run the model for our period of study.

7.3 Results

Figure 7-1 presents the STWAVE+ output for H_s, T_p, and D_p for all values of the friction coefficients (C_f) compared to the ADCP record. For H_s, it is noted that even for C_f = 0.000 (no friction), the STWAVE+ model run tends to underpredict the ADCP waves heights during the peaks of the two storms (~2 m). Conversely, the model tends to overpredict the ADCP measurements when waves are smaller (0.5-1.0 m). The reason for this behavior is presently unclear. However, under smaller wave conditions, the results for all friction values tend to cluster together, and distinctly separate during the storms, as should be expected from Eq. (4).

The middle panel in Figure 7-1 shows the peak wave period (Tp) for the STWAVE+ outputs versus the ADCP measurements. The ADCP data is quite noisy, much more so than the measurements from NDBC-41112 in Figure 4-4. In general, the ADCP varies between 5 and 10 seconds, whereas the STWAVE+ output consistently stays within 7 and 9 seconds.

Finally for the bottom panel in Figure 7-1, the peak wave direction varies between 180 and 270 degrees for the ADCP data, whereas the STWAVE+ results trend along 270 to 315 degrees. This could be attributed to the half-plane limitations of STWAVE+, and that offshore winds are not taken into account.

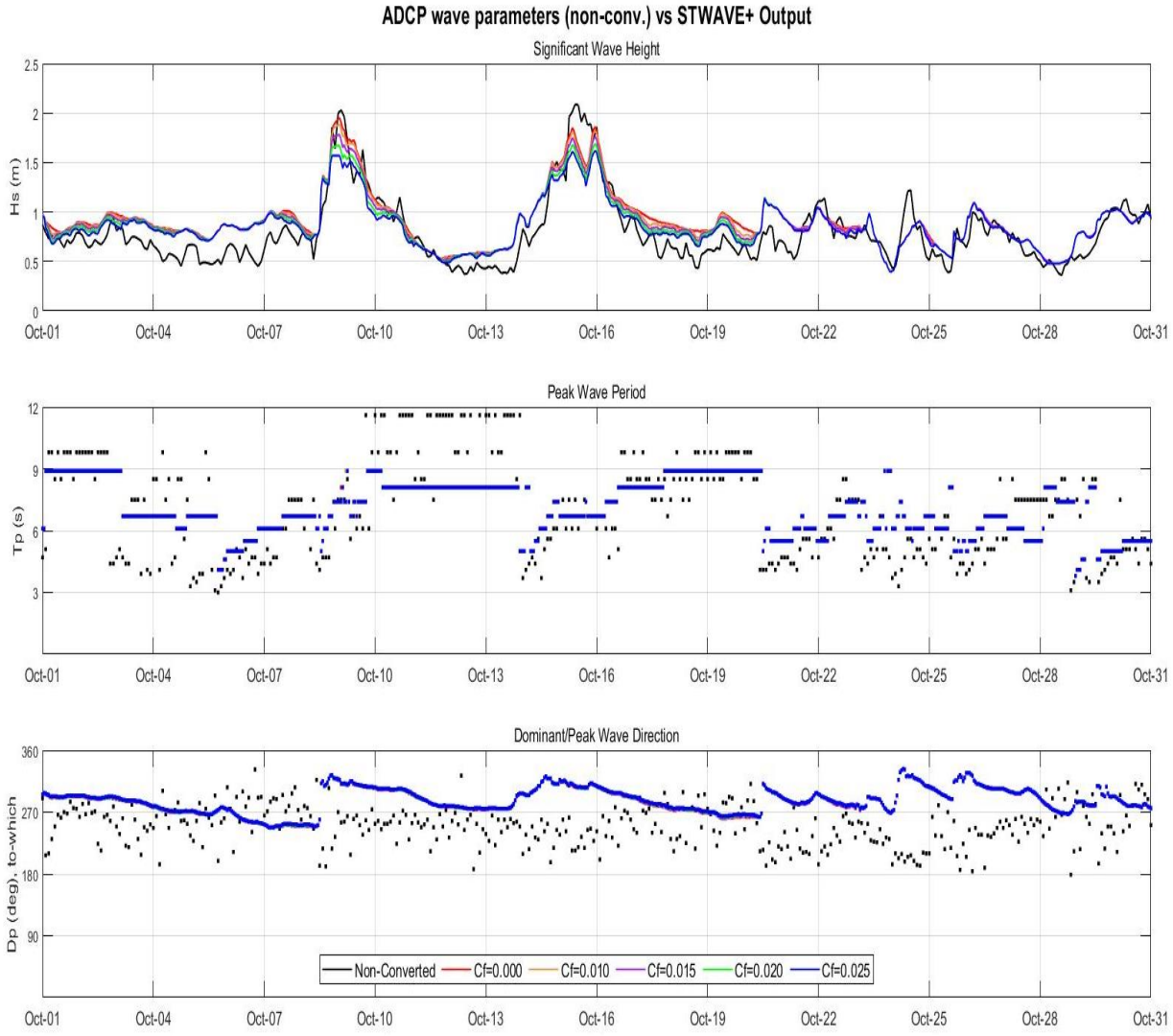

Figure 7-1 STWAVE+ model output wave parameters

7.4 Selection of the Best-Fit Friction Factor

Regardless of the issues raised above, a method for selecting the best value for C_f can still be demonstrated. Firstly, scatter plots were produced to visualize the overall performance for each run, and error metrics were calculated (Figure 7-2). These plots confirm that STWAVE+ tends to overpredict when the ADCP reports smaller waves, and underpredict the larger waves. As seen, the error metrics do not differ significantly, although, although 0.015 and 0.020 tend to be the best candidates.

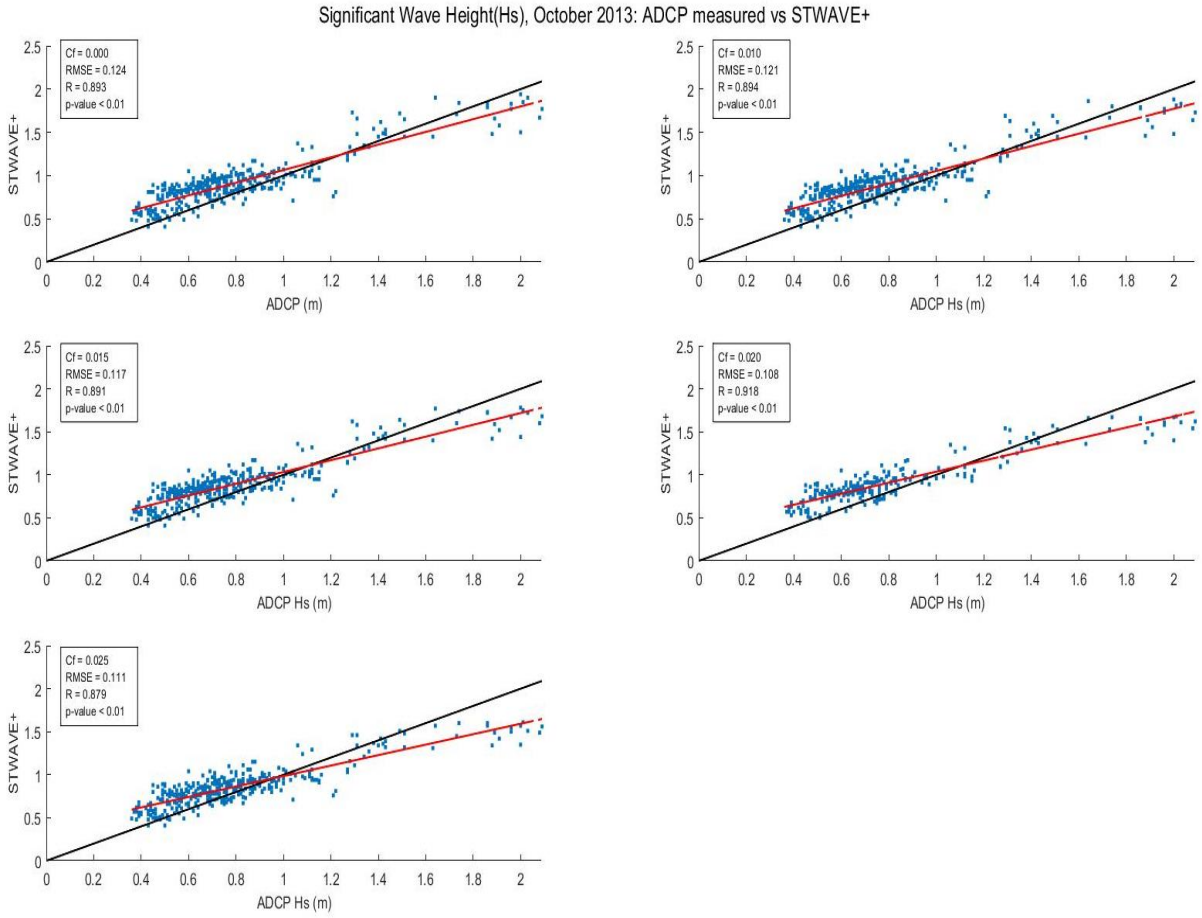

Figure 7-2 Scatter plots of half-plane STWAVE+ results for different values of Cf versus full-plane ADCP measurements. The solid black lines represent perfect agreement, and the red lines are linear best-fits.

The final step in the methodology is to construct Quantile-Quantile plots for the results for each friction coefficient scenario against the measured data (Figure 7-3).

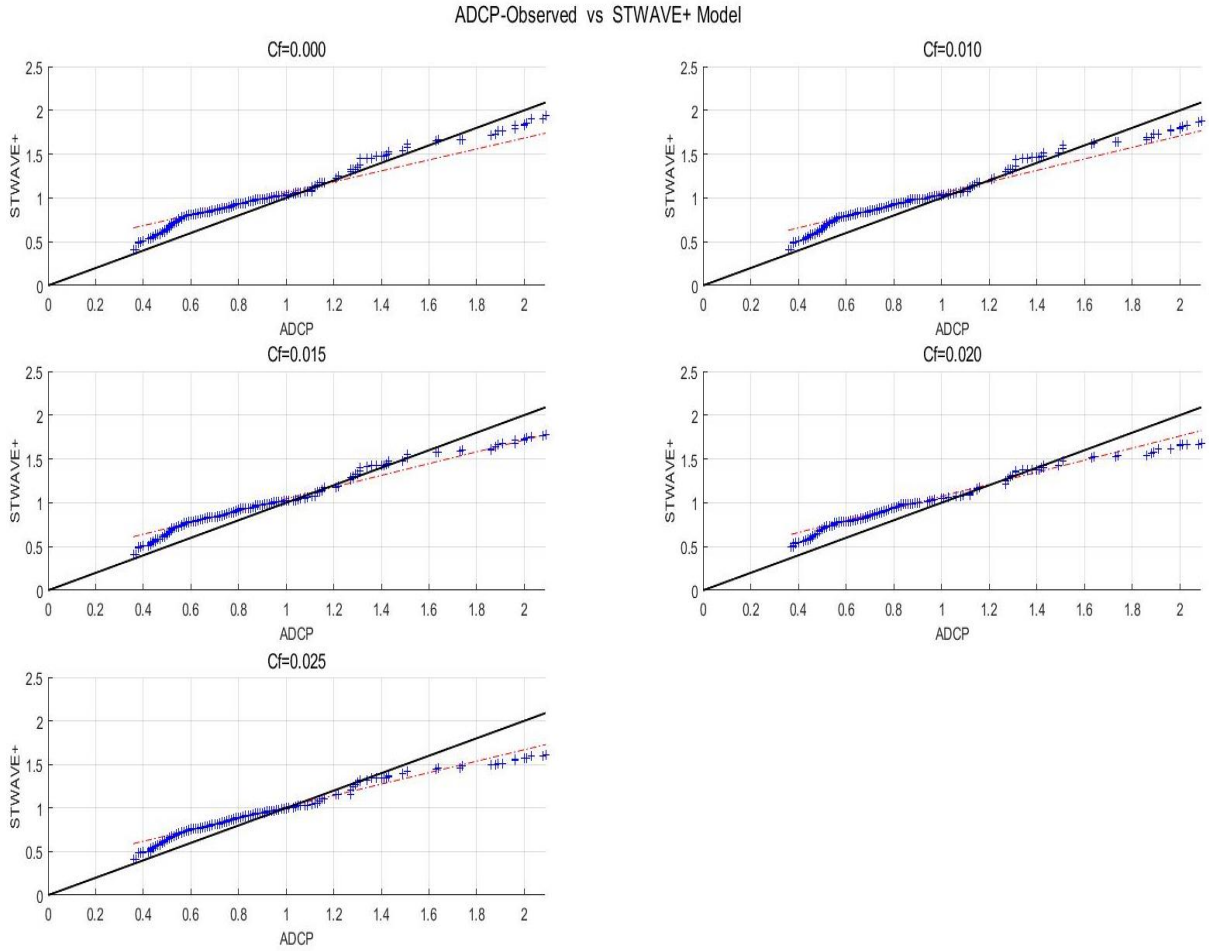

Figure 7-3 Quantile-Quantile plots of half-plane STWAVE+ results for different values of Cf, versus full-plane ADCP measurements.

In Figure 7-3, it is apparent that for the highest waves, no friction seems to fit best (C_f =0.0). This result, in conjunction with the significant underprediction of OWI-7611 to NDBC-41112 during the two October storms, as seen in Figure 4-4, would lead one to believe that the main problem may lie with the veracity of the offshore input conditions at OWI-7203, *i.e.* that the JONSWAP friction model, along with adopting the default value for its friction coefficient, had already dissipated too much wave energy before reaching the outer boundary of the STWAVE+ model. Even at the depth of 24.5 m, linear theory predicts waves with periods as

short as 5.6 s are entering intermediate depth, where they begin to feel the bed. On the other hand, it is perplexing that OWI-7611 appears to track the time series of Hs measured by NDBC-41112 for small waves as seen in Figure 4-5, whereas the STWAVE+ results are clearly overpredicting the heights of the smaller waves, regardless of the value of C_f. Unfortunately, no wave measurements taken near OWI-7203 are available to test this hypothesis.

CHAPTER 8

Summary and Conclusion

The motivation behind this study is to reach a model to simulate nearshore wave data for the Mayport in Florida. This is because like many other nearshore regions, there is no real long term wave data for the Mayport to be used by practitioners. Thus, a synthetic wave record is required. Some tools were utilized to reach the desired output. First, whereas real-time offshore data was not available intensively, an offshore buoy in the vicinity had some wave data recording. This data was used by Oceanweather incorporated (OWI) as the hindcast data to develop and validate a model to simulate and forecast offshore wave data. The produced data by OWI was utilized as the platform to work on. This is where STWAVE+ came into play. STWAVE+ transforms far offshore data to a nearshore type that relies on the concept of incorporating a bed friction coefficient (C_f). In other words, as the far offshore waves propagate toward the shore, they lose energy due to the bed friction, which converts to nearshore waves. This insight was put into practice and a variety of bed friction coefficients (C_f) were implemented. The STWAVE+ generated results were compared with real-time nearshore wave data. The nearshore source was an Acoustic Doppler Current Profiler (ADCP) directional wave instrument deployed 3 km offshore of Mayport, FL at a mean water depth of 9.5 m. Bed frictions coefficients (C_f) ranging from no friction (0.00) and 0.010 to 0.025 with the increment of 0.005 were incorporated into the STWAVE+ model. The output results were analyzed through a three-pronged approach to in order to calibrate the wave transformation models for energy losses due to bottom friction: 1) direct comparison of the time series of energy-based significant wave height (Hs) from the model at the location of a nearshore wave gauge, using a range of realistic values for the bed friction coefficient, 2) examination of scatter plots

constructed between the measured data and model results, and 3) utilization of Quantile-Quantile analyses. After doing these analyses, it was concluded that 0.015 is the best choice to calibrate the nearshore wave model in the Mayport.

APPENDIX A

OWI-7611 Hindcast vs NDBC-41112 Measured Time Series Plots for The Wave Parameters for Each Month

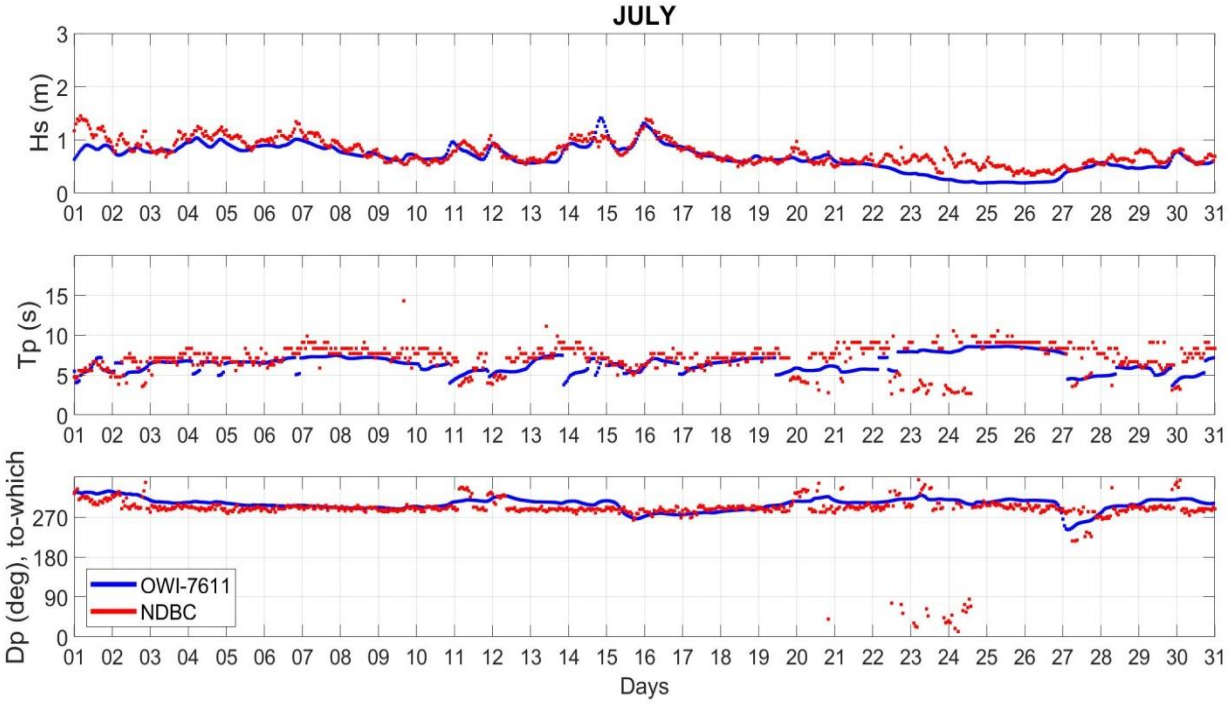

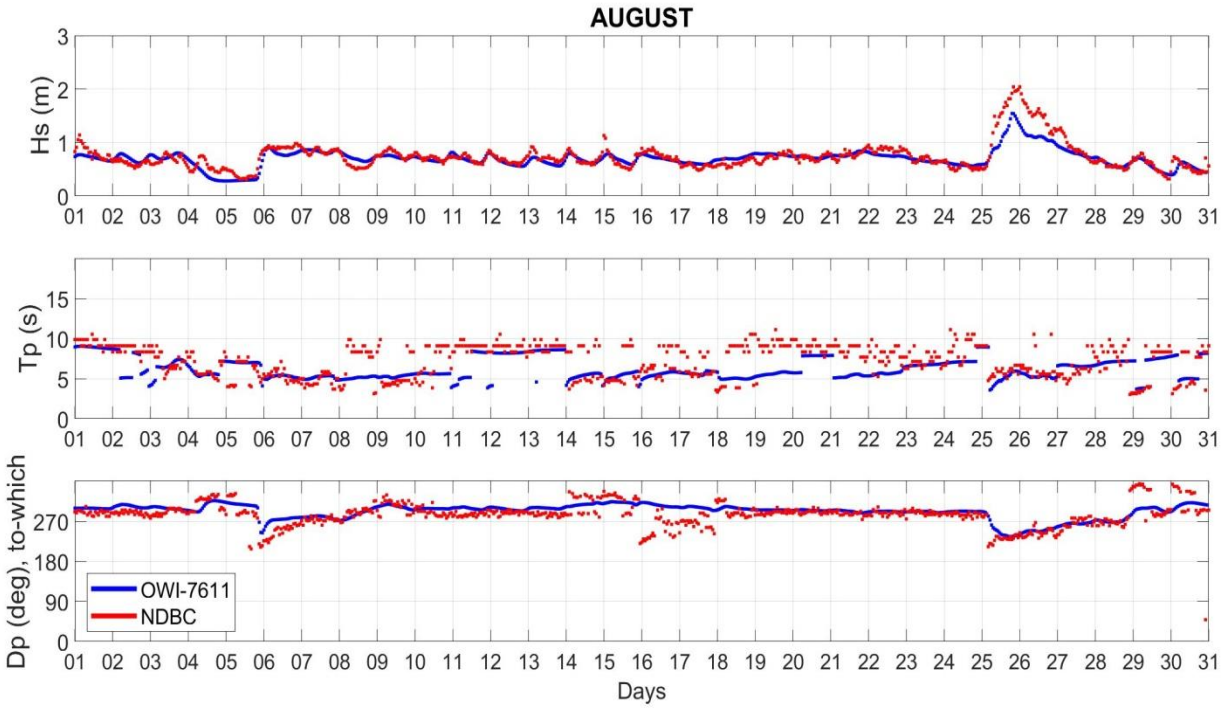
AUGUST
Hs (m)
Tp (s)
Dp (deg), to-which
OWI-7611
NDBC
Days

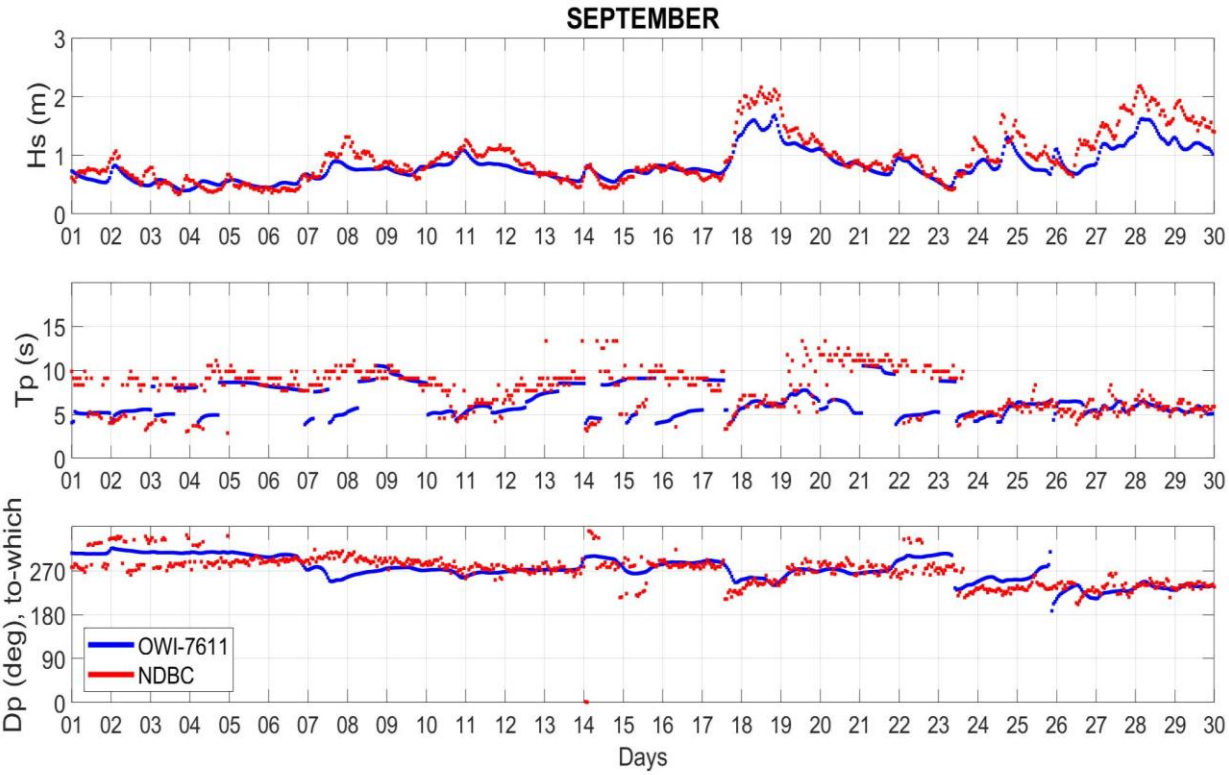
SEPTEMBER
Hs (m)
Tp (s)
Dp (deg), to-which
OWI-7611
NDBC
Days

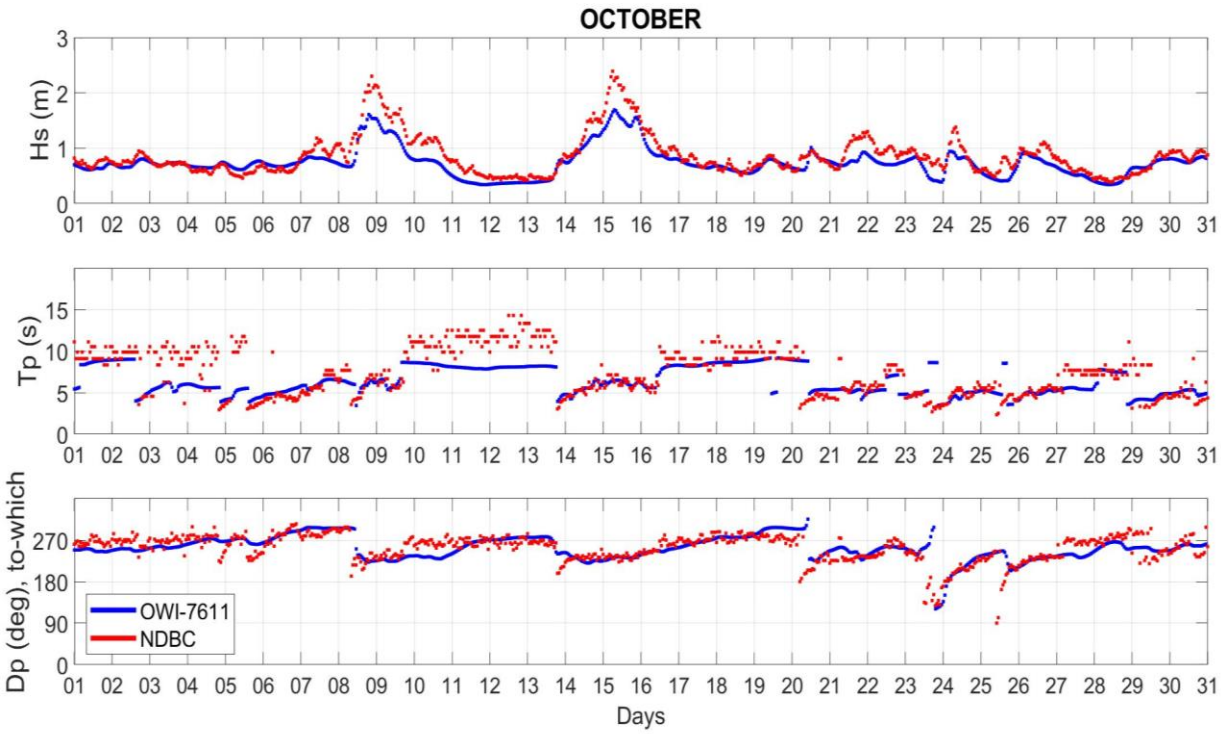
OCTOBER
Hs (m)
Tp (s)
Dp (deg), to-which
OWI-7611
NDBC
Days

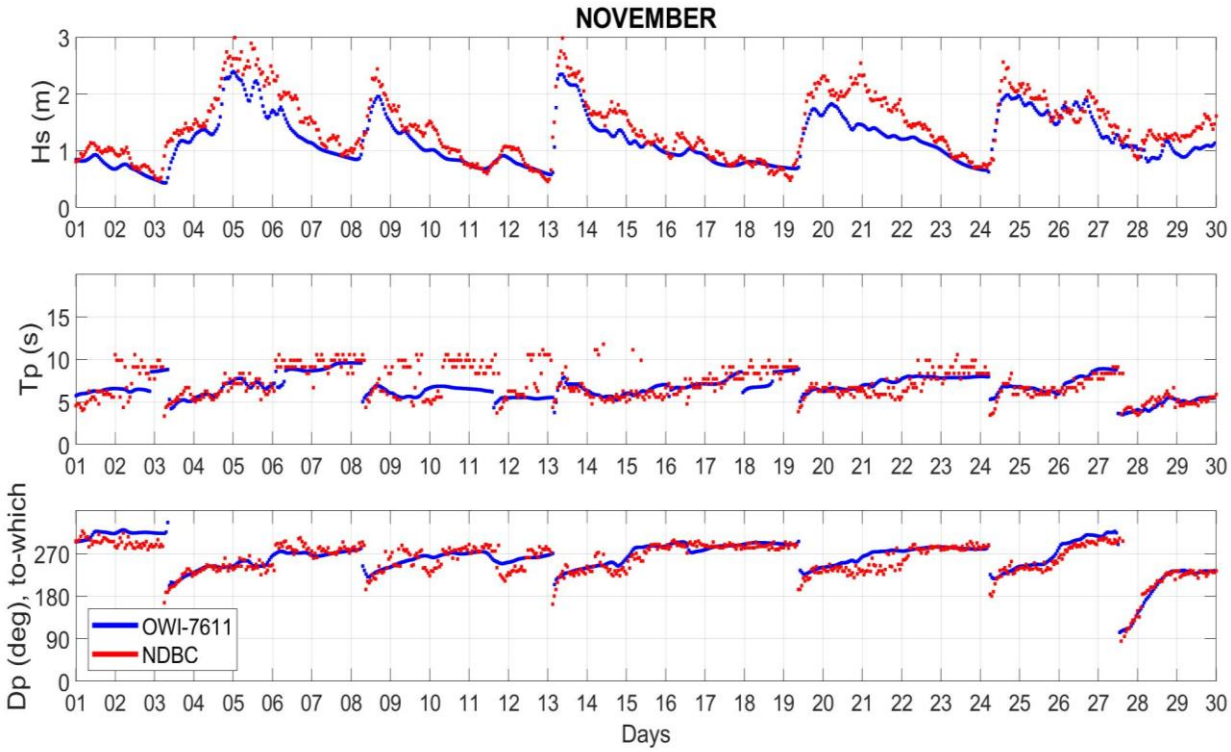
NOVEMBER
Hs (m)
Tp (s)
Dp (deg), to-which
OWI-7611
NDBC
Days

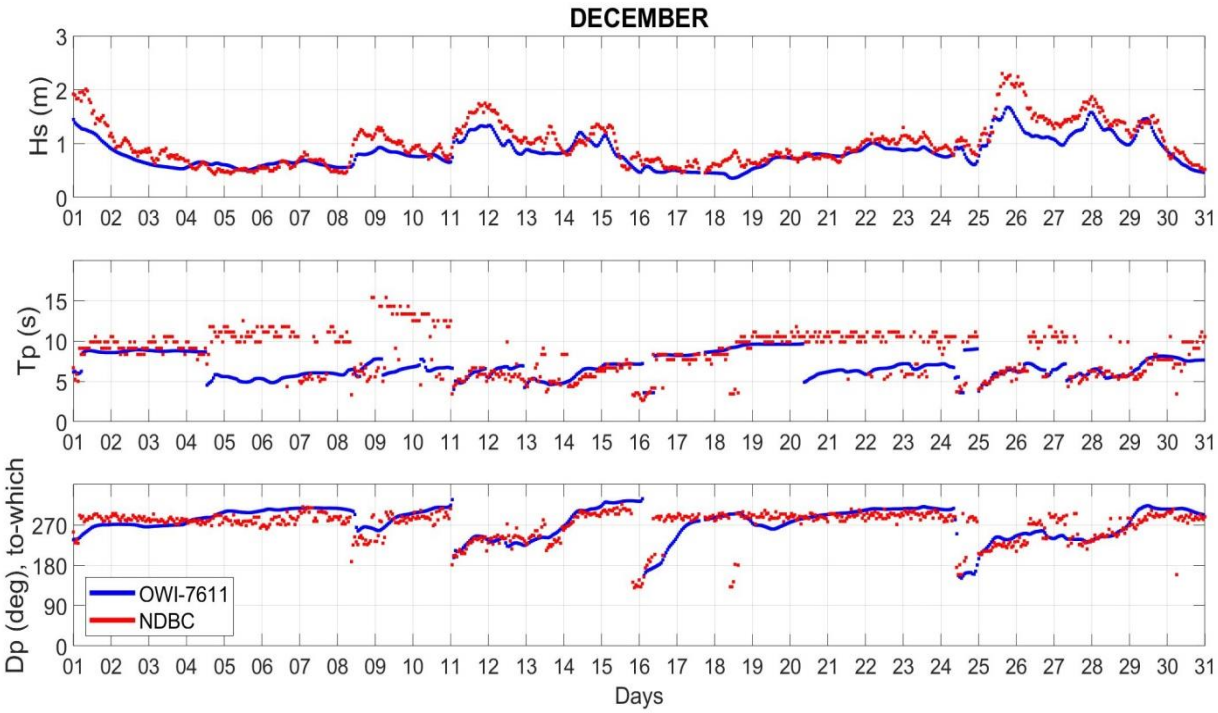
DECEMBER
Hs (m)
Tp (s)
Dp (deg), to-which
OWI-7611
NDBC
Days

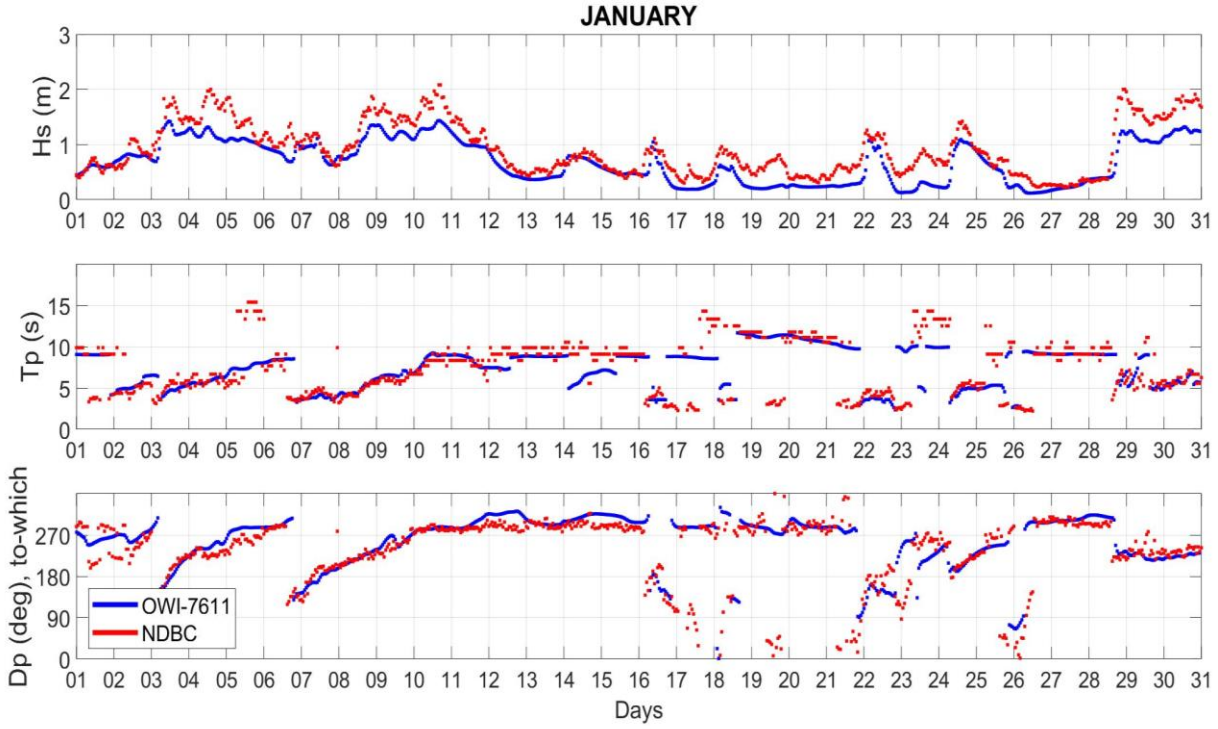
JANUARY
Hs (m)
Tp (s)
Dp (deg), to-which
OWI-7611
NDBC
Days

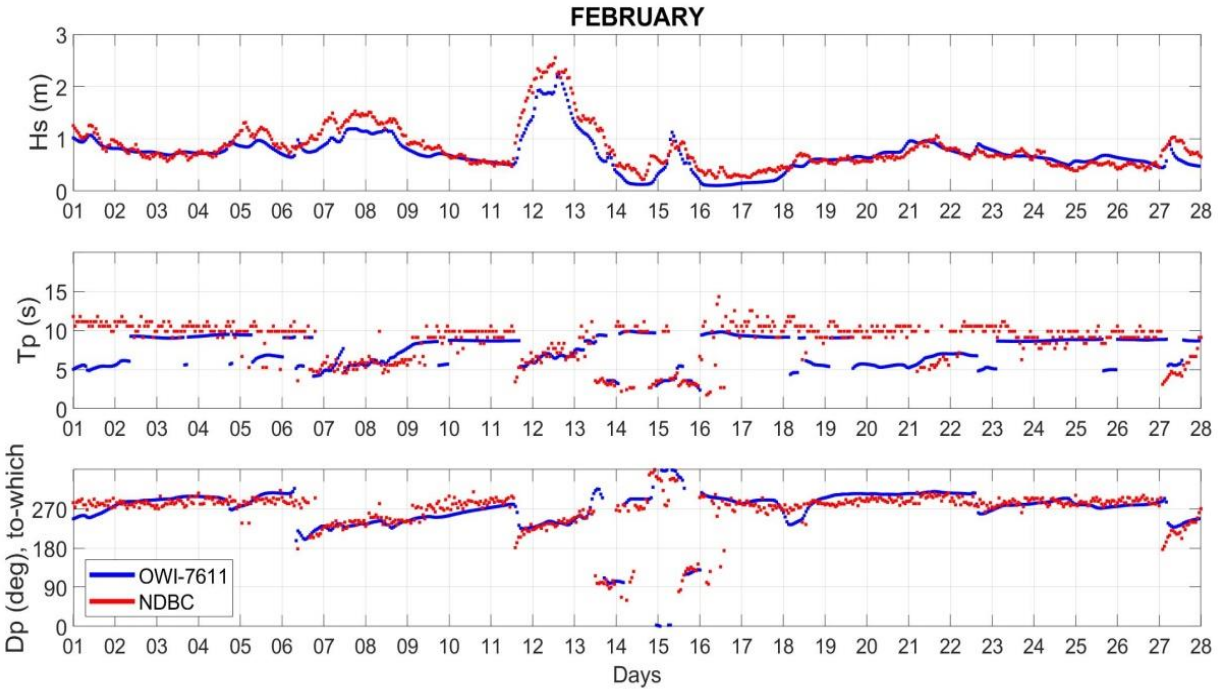
FEBRUARY
Hs (m)
Tp (s)
Dp (deg), to-which
OWI-7611
NDBC
Days

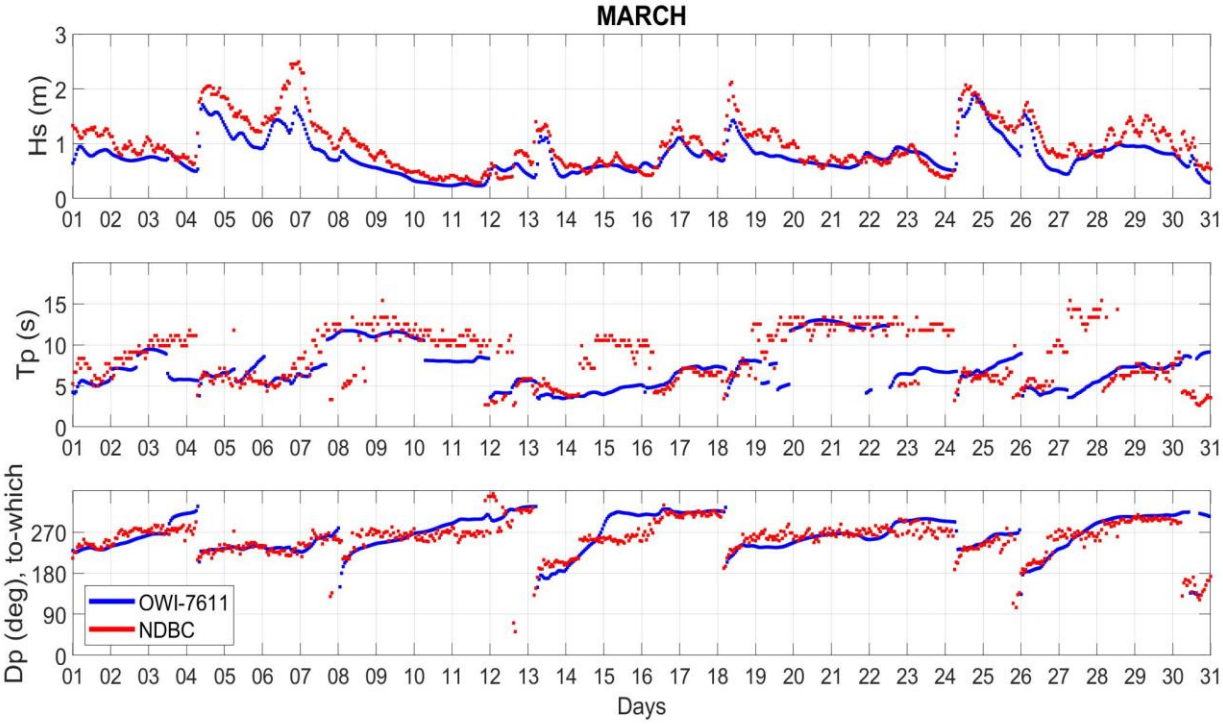
MARCH
Hs (m)
Tp (s)
Dp (deg), to-which
OWI-7611
NDBC
Days

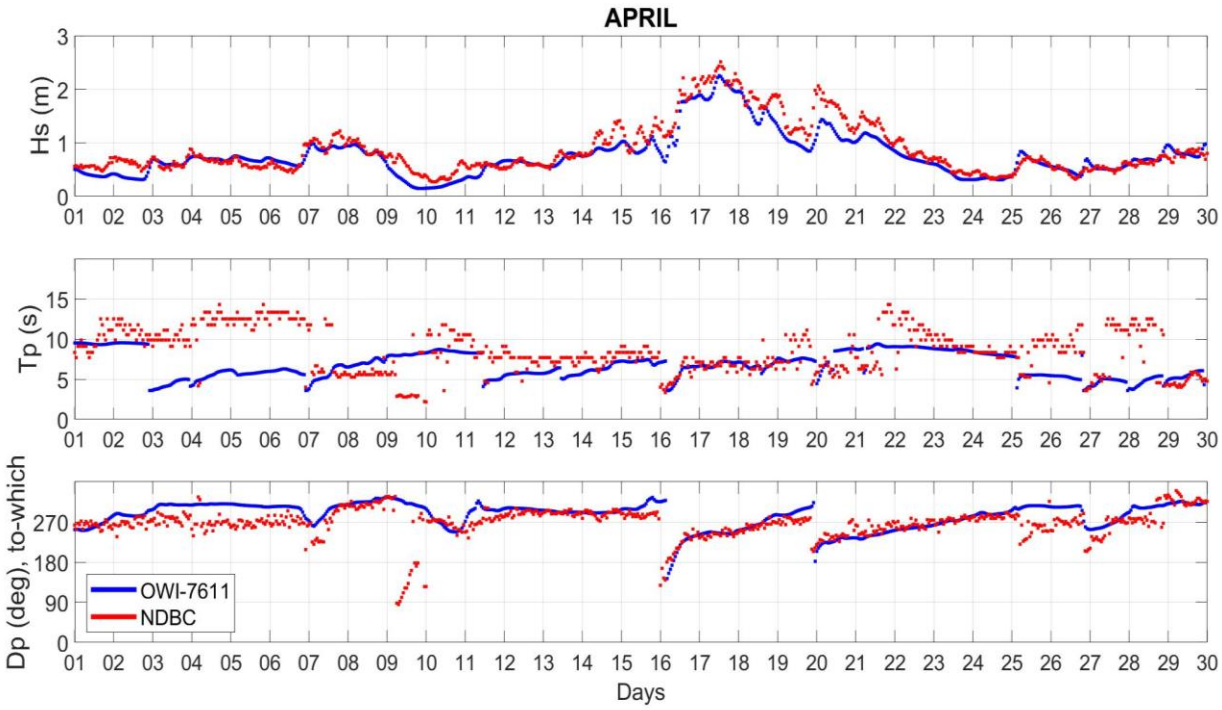
APRIL
Hs (m)
Tp (s)
Dp (deg), to-which
OWI-7611
NDBC
Days

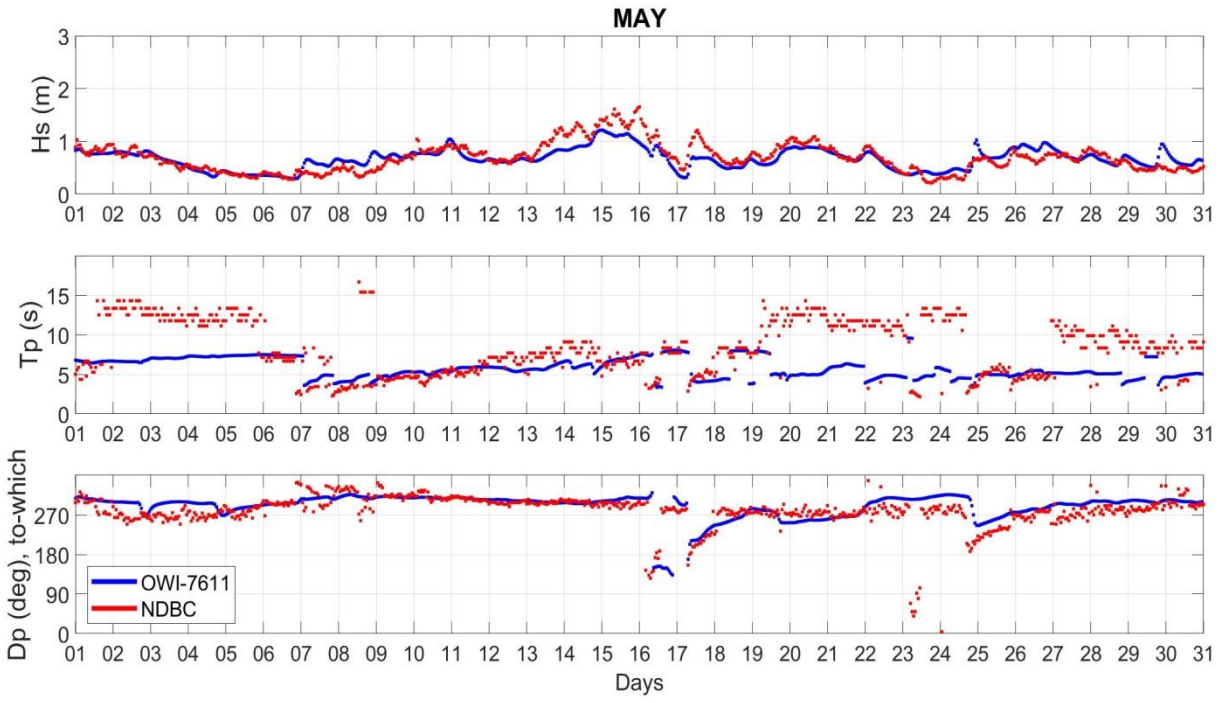
MAY
Hs (m)
Tp (s)
Dp (deg), to-which
OWI-7611
NDBC
Days

APPENDIX B

10-Day Significant Wave Height Plots: OWI-7611, NDBC (CDIP-132), and ADCP Pressure & Surface Tracking with Instrument at 1m Elevation

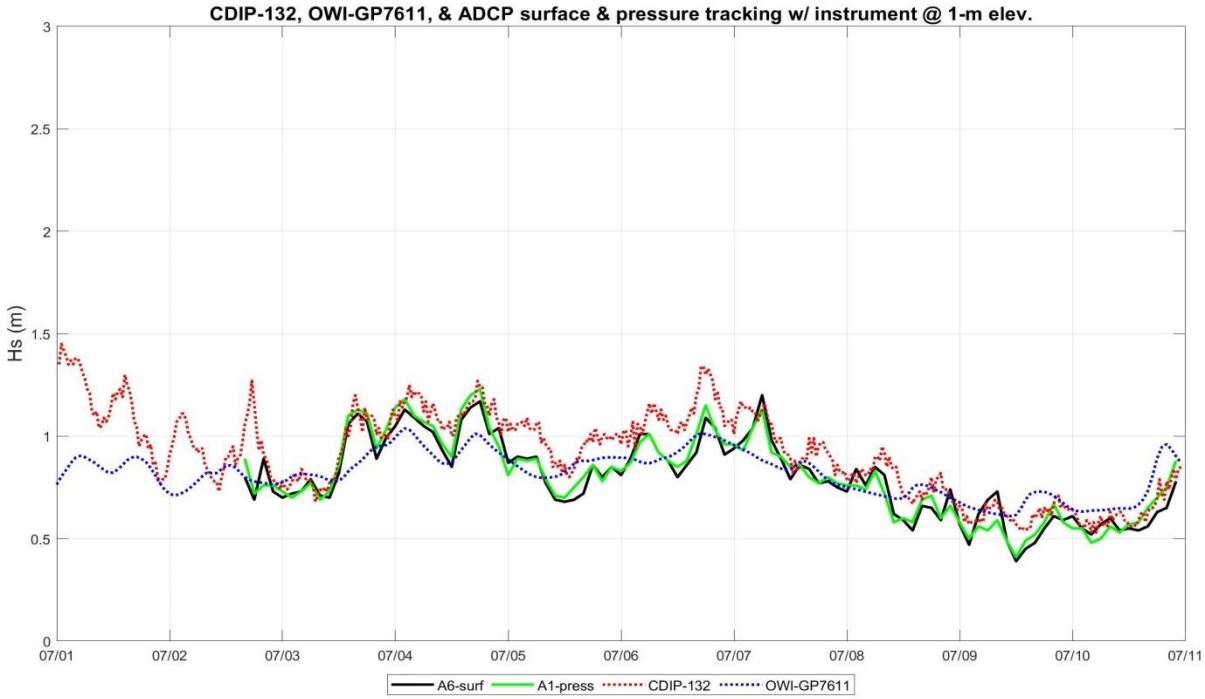

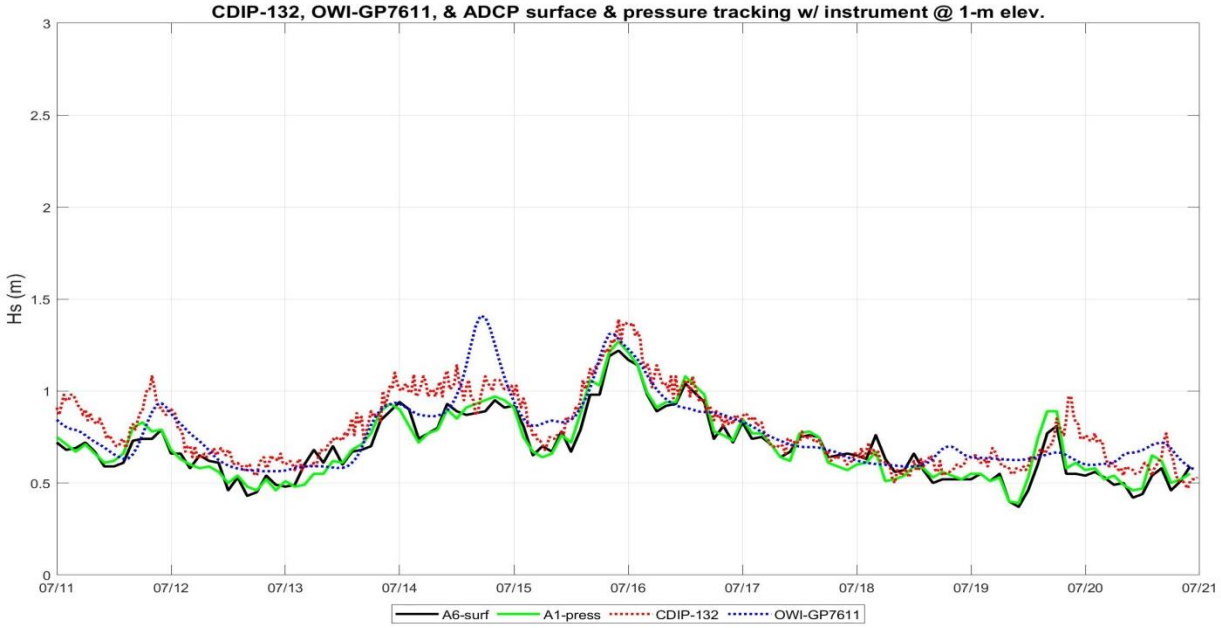
CDIP-132, OWI-GP7611, & ADCP surface & pressure tracking w/ instrument @ 1-m elev.
Hs (m)
3
2.5
2
1.5
1
0.5
0
07/11
07/12
07/13
07/14
07/15
07/16
07/17
07/18
07/19
07/20
07/21
A6-surf
A1-press
CDIP-132
OWI-GP7611

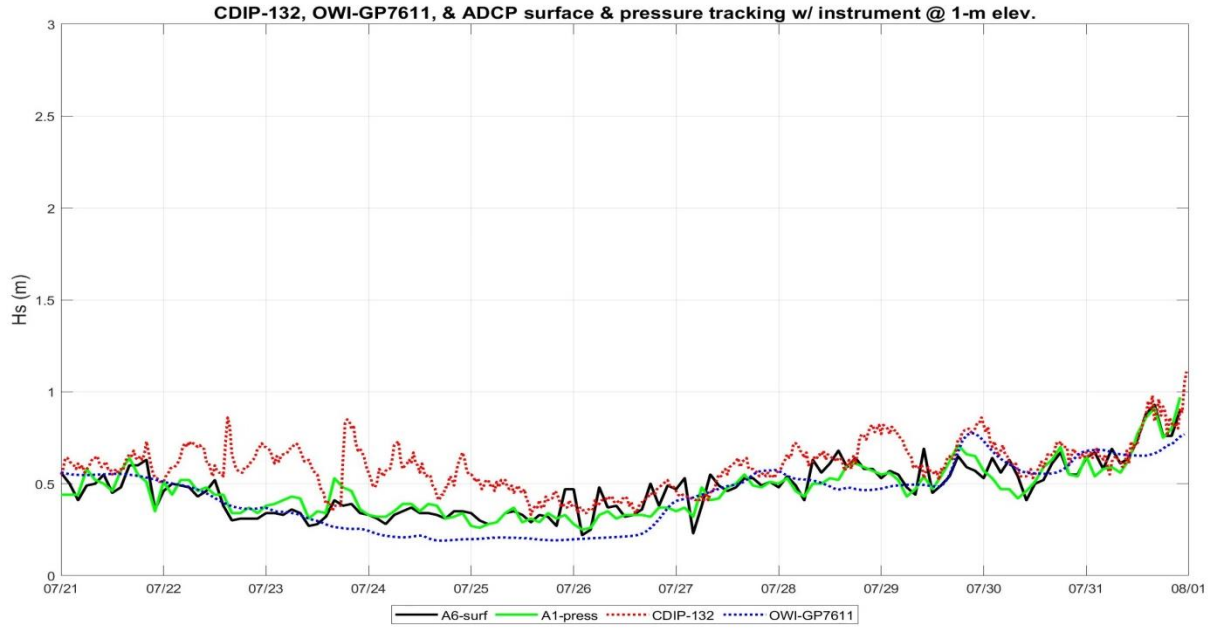
CDIP-132, OWI-GP7611, & ADCP surface & pressure tracking w/ instrument @ 1-m elev.
Hs (m)
3
2.5
2
1.5
1
0.5
0
07/21
07/22
07/23
07/24
07/25
07/26
07/27
07/28
07/29
07/30
07/31
08/01
A6-surf
A1-press
CDIP-132
OWI-GP7611

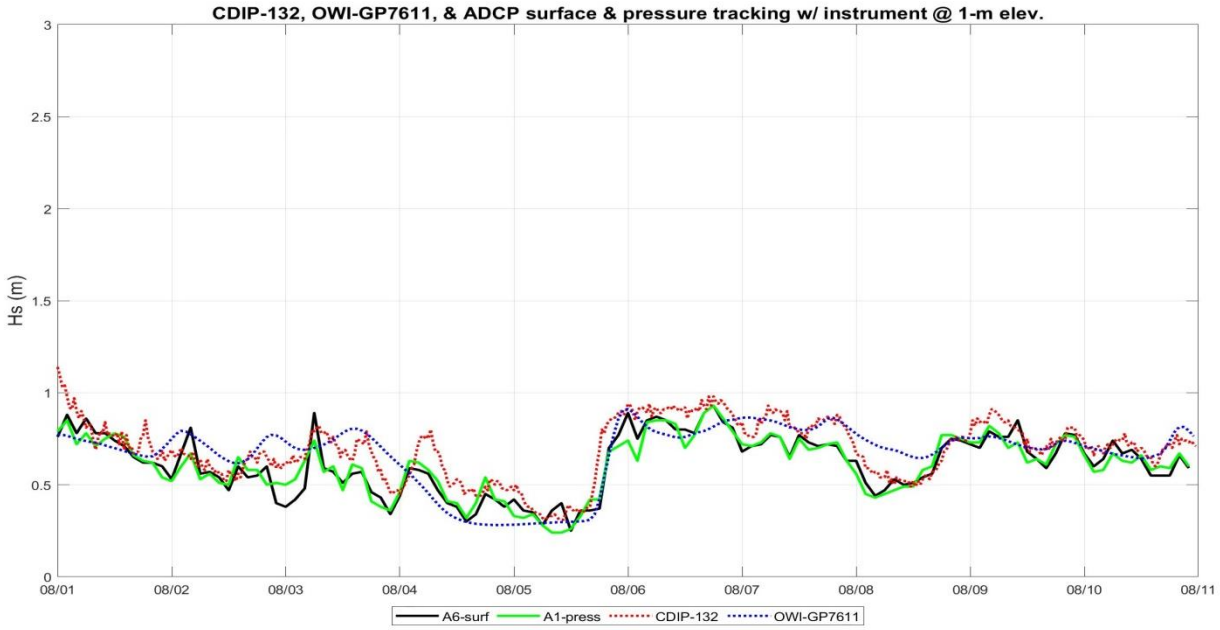
CDIP-132, OWI-GP7611, & ADCP surface & pressure tracking w/ instrument @ 1-m elev.
Hs (m)
3
2.5
2
1.5
1
0.5
0
08/01
08/02
08/03
08/04
08/05
08/06
08/07
08/08
08/09
08/10
08/11
A6-surf
A1-press
CDIP-132
OWI-GP7611

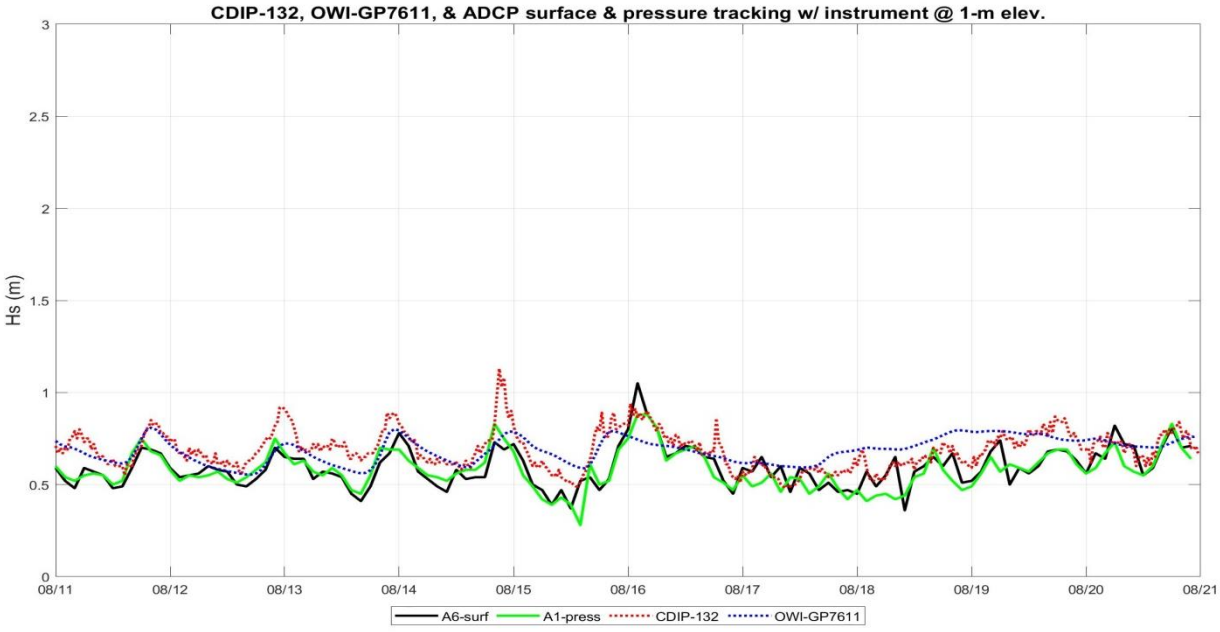
CDIP-132, OWI-GP7611, & ADCP surface & pressure tracking w/ instrument @ 1-m elev.
Hs (m)
3
2.5
2
1.5
1
0.5
0
08/11
08/12
08/13
08/14
08/15
08/16
08/17
08/18
08/19
08/20
08/21
A6-surf
A1-press
CDIP-132
OWI-GP7611

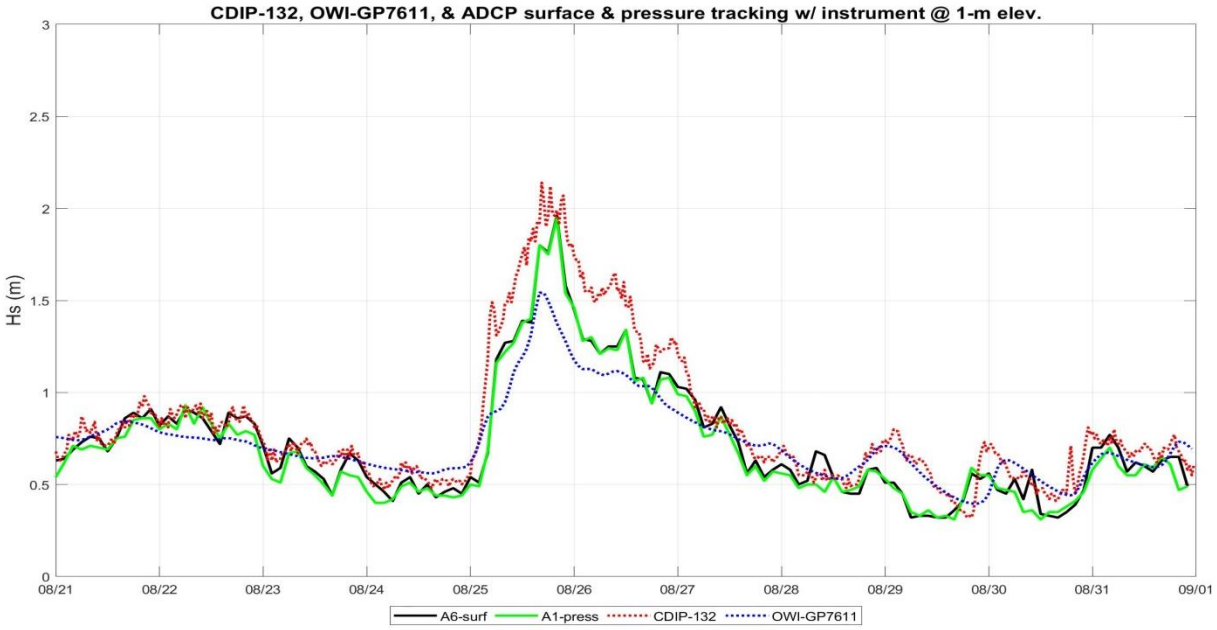
CDIP-132, OWI-GP7611, & ADCP surface & pressure tracking w/ instrument @ 1-m elev.
Hs (m)
0
0.5
1
1.5
2
2.5
3
08/21
08/22
08/23
08/24
08/25
08/26
08/27
08/28
08/29
08/30
08/31
09/01
A6-surf
A1-press
CDIP-132
OWI-GP7611

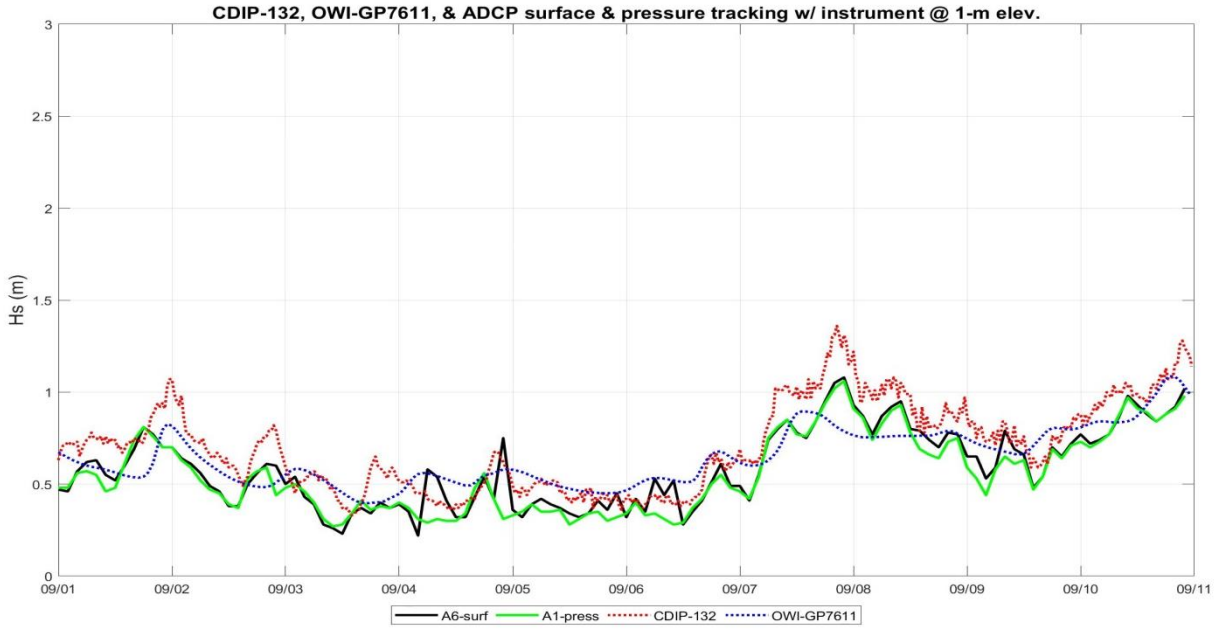
CDIP-132, OWI-GP7611, & ADCP surface & pressure tracking w/ instrument @ 1-m elev.
Hs (m)
0
0.5
1
1.5
2
2.5
3
09/01
09/02
09/03
09/04
09/05
09/06
09/07
09/08
09/09
09/10
09/11
A6-surf
A1-press
CDIP-132
OWI-GP7611

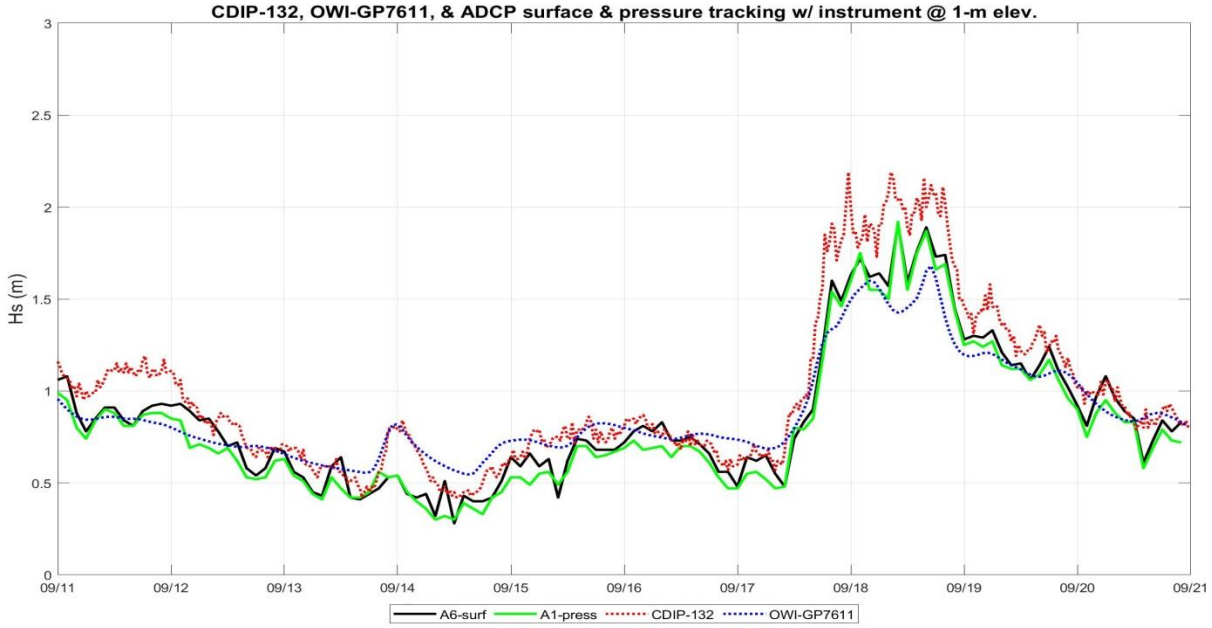
CDIP-132, OWI-GP7611, & ADCP surface & pressure tracking w/ instrument @ 1-m elev.
Hs (m)
3
2.5
2
1.5
1
0.5
0
09/11
09/12
09/13
09/14
09/15
09/16
09/17
09/18
09/19
09/20
09/21
A6-surf
A1-press
CDIP-132
OWI-GP7611

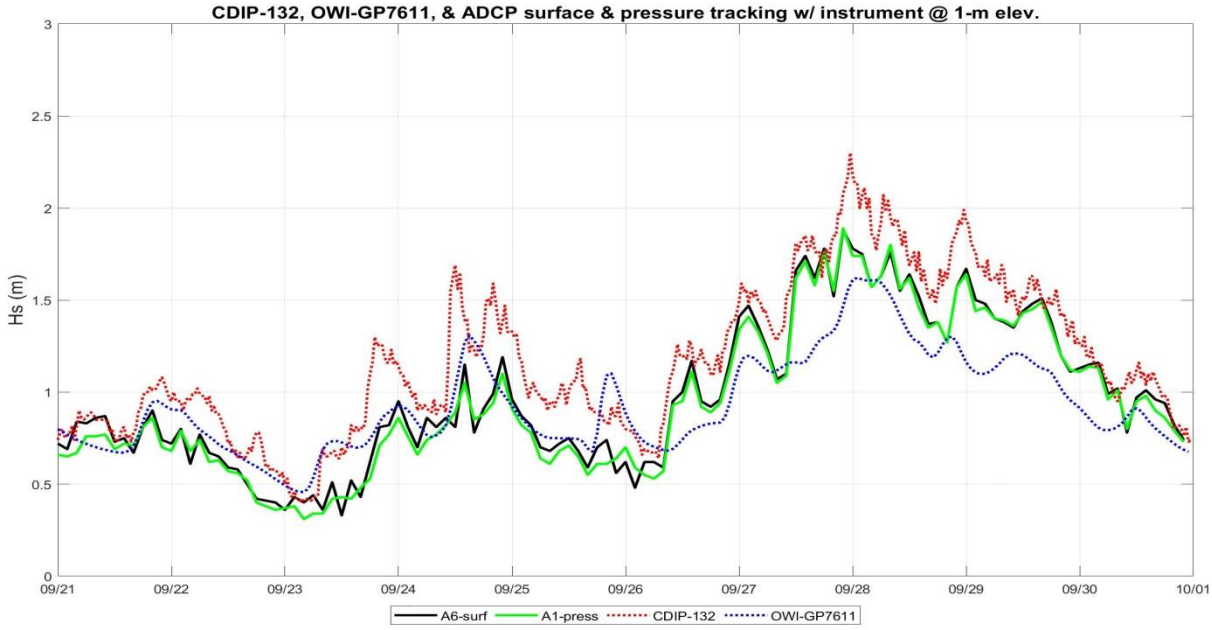
CDIP-132, OWI-GP7611, & ADCP surface & pressure tracking w/ instrument @ 1-m elev.
Hs (m)
3
2.5
2
1.5
1
0.5
0
09/21
09/22
09/23
09/24
09/25
09/26
09/27
09/28
09/29
09/30
10/01
A6-surf
A1-press
CDIP-132
OWI-GP7611

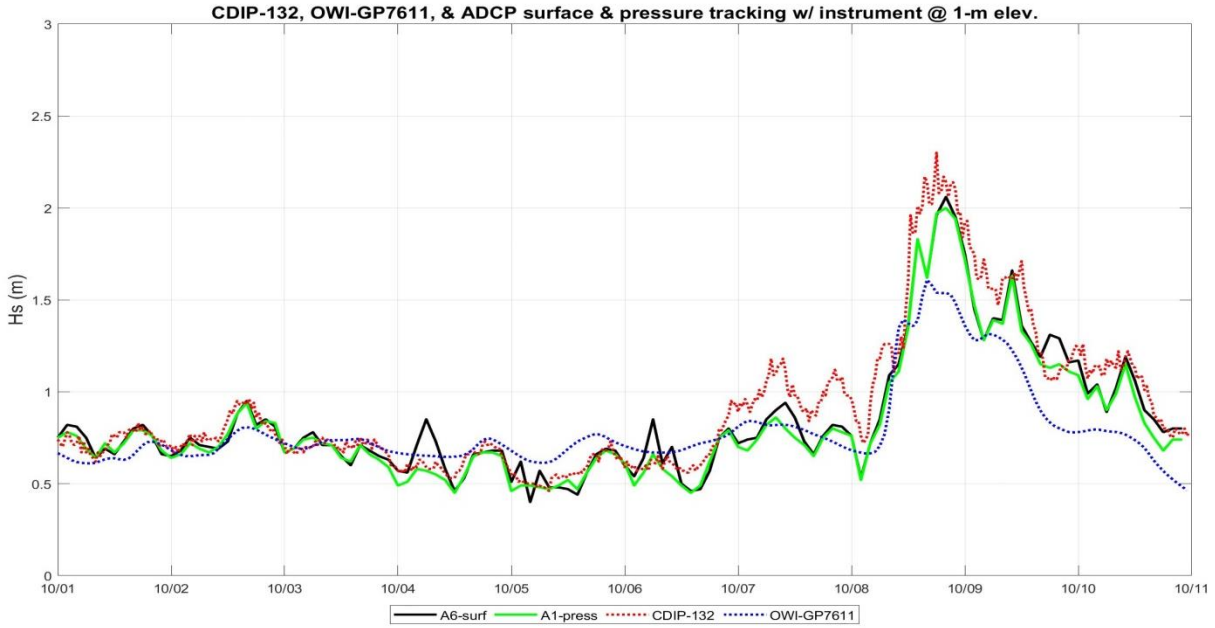
CDIP-132, OWI-GP7611, & ADCP surface & pressure tracking w/ instrument @ 1-m elev.
Hs (m)
0
0.5
1
1.5
2
2.5
3
10/01
10/02
10/03
10/04
10/05
10/06
10/07
10/08
10/09
10/10
10/11
A6-surf
A1-press
CDIP-132
OWI-GP7611

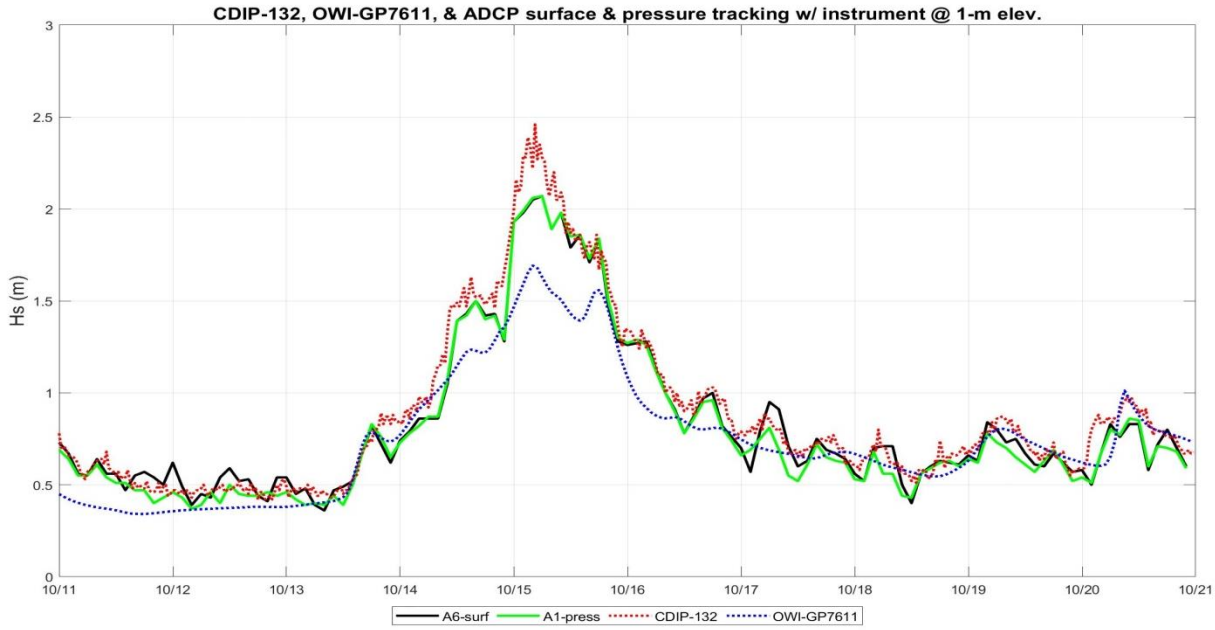
CDIP-132, OWI-GP7611, & ADCP surface & pressure tracking w/ instrument @ 1-m elev.
Hs (m)
0
0.5
1
1.5
2
2.5
3
10/11
10/12
10/13
10/14
10/15
10/16
10/17
10/18
10/19
10/20
10/21
A6-surf
A1-press
CDIP-132
OWI-GP7611

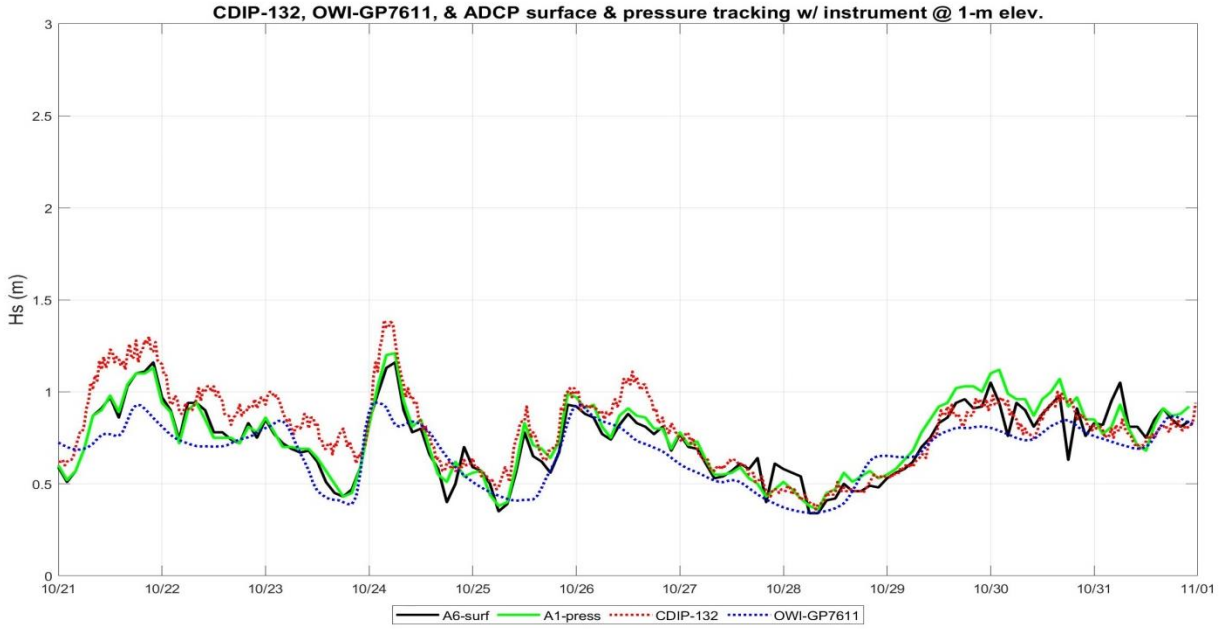
CDIP-132, OWI-GP7611, & ADCP surface & pressure tracking w/ instrument @ 1-m elev.
Hs (m)
0
0.5
1
1.5
2
2.5
3
10/21
10/22
10/23
10/24
10/25
10/26
10/27
10/28
10/29
10/30
10/31
11/01
A6-surf
A1-press
CDIP-132
OWI-GP7611

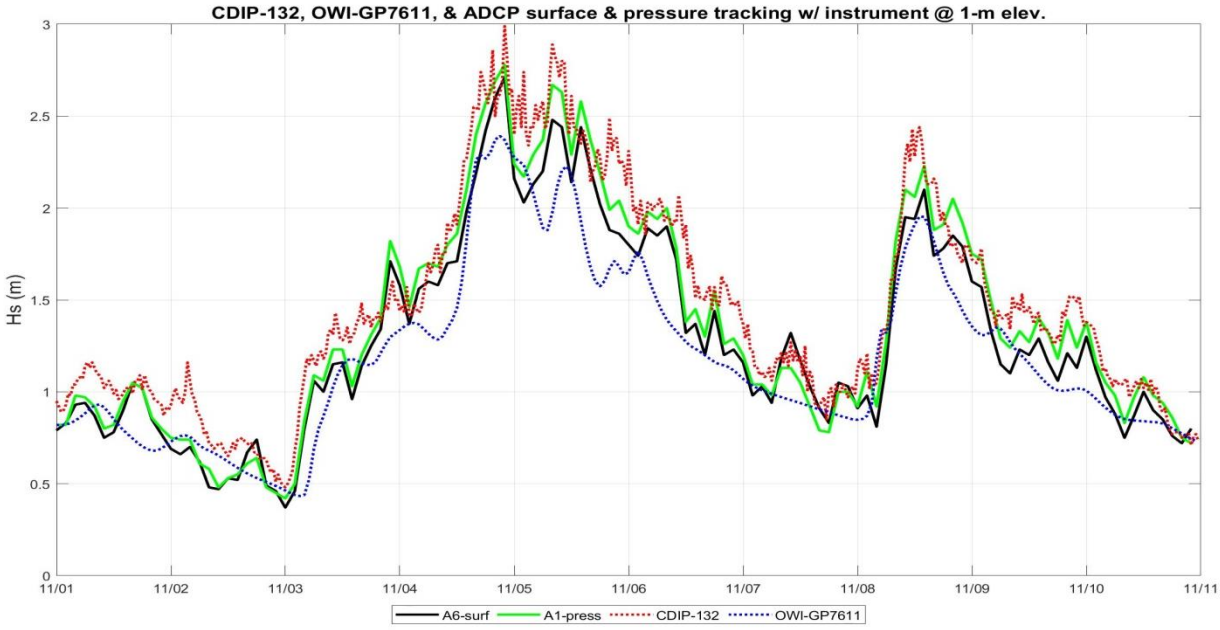
CDIP-132, OWI-GP7611, & ADCP surface & pressure tracking w/ instrument @ 1-m elev.
Hs (m)
0
0.5
1
1.5
2
2.5
3
11/01
11/02
11/03
11/04
11/05
11/06
11/07
11/08
11/09
11/10
11/11
A6-surf
A1-press
CDIP-132
OWI-GP7611


CDIP-132, OWI-GP7611, & ADCP surface & pressure tracking w/ instrument @ 1-m elev.
Hs (m)
0
0.5
1
1.5
2
2.5
3
11/11
11/12
11/13
11/14
11/15
11/16
11/17
11/18
11/19
11/20
11/21
A6-surf
A1-press
CDIP-132
OWI-GP7611

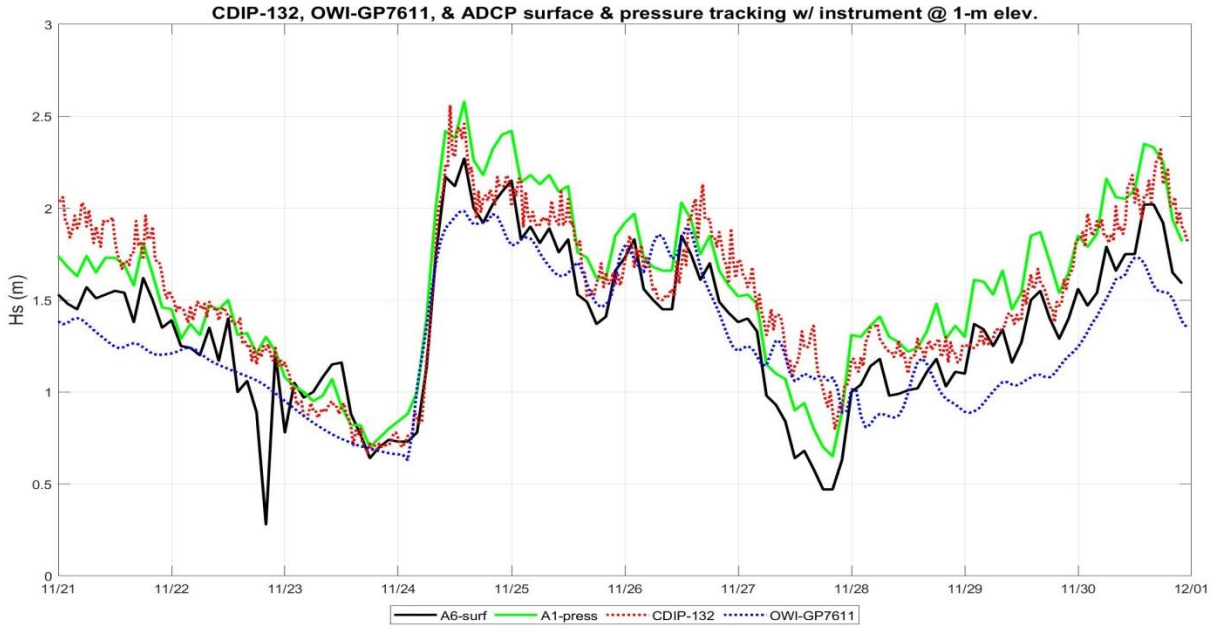
CDIP-132, OWI-GP7611, & ADCP surface & pressure tracking w/ instrument @ 1-m elev.
Hs (m)
0
0.5
1
1.5
2
2.5
3
11/21
11/22
11/23
11/24
11/25
11/26
11/27
11/28
11/29
11/30
12/01
A6-surf
A1-press
CDIP-132
OWI-GP7611

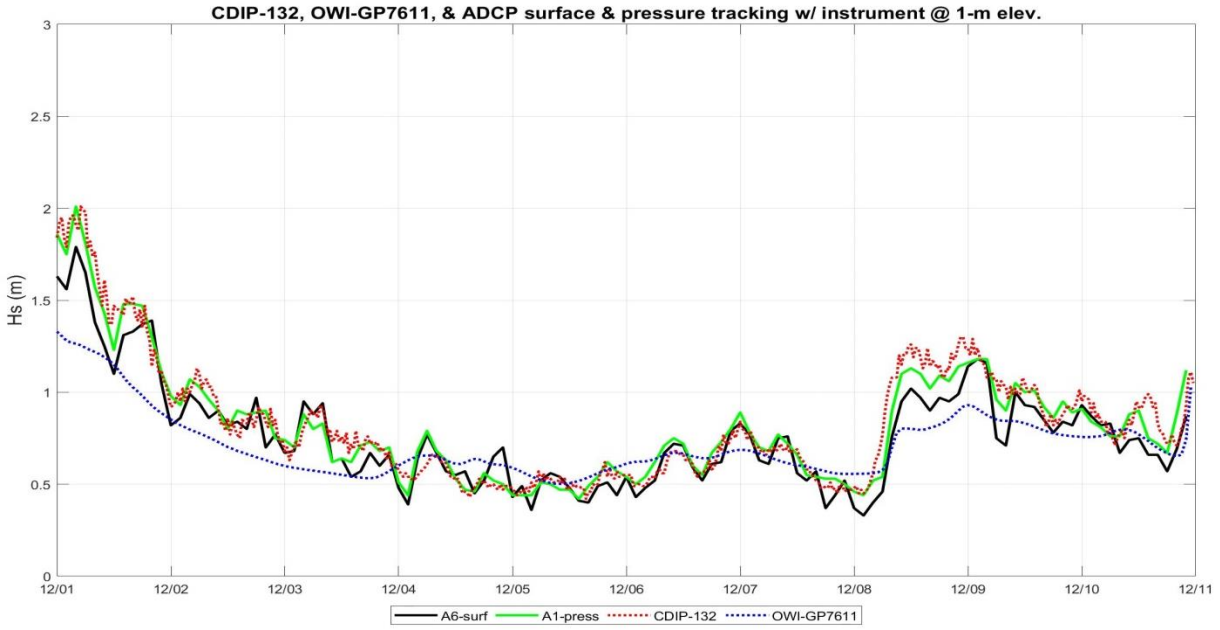
CDIP-132, OWI-GP7611, & ADCP surface & pressure tracking w/ instrument @ 1-m elev.
Hs (m)
3
2.5
2
1.5
1
0.5
0
12/01
12/02
12/03
12/04
12/05
12/06
12/07
12/08
12/09
12/10
12/11
A6-surf
A1-press
CDIP-132
OWI-GP7611

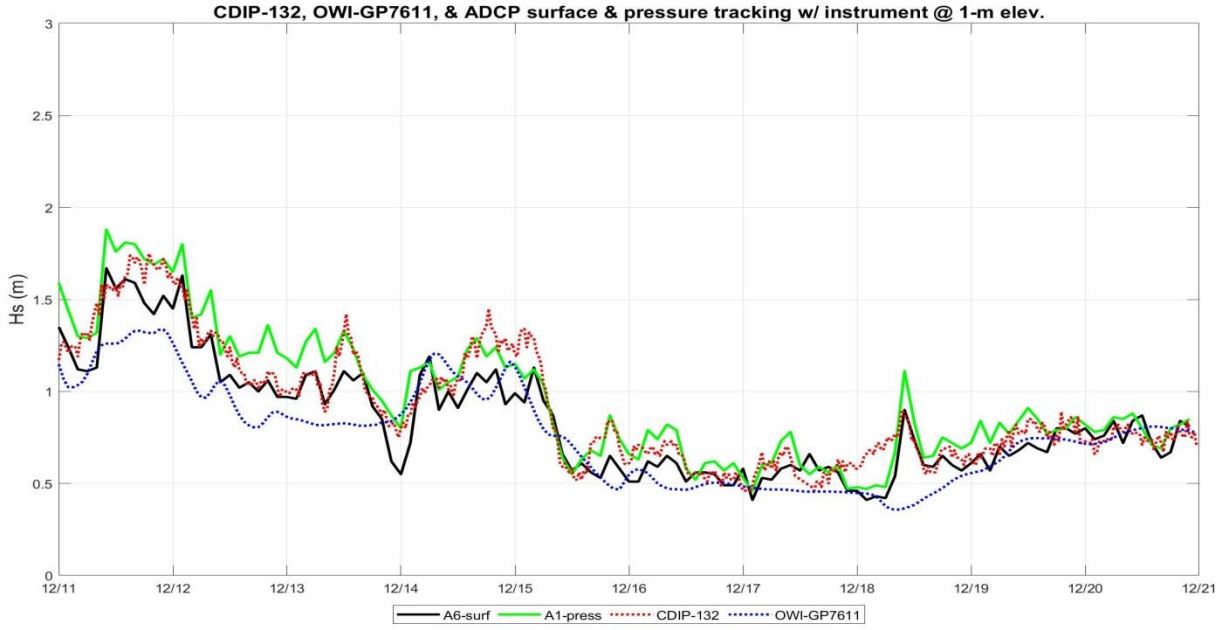
CDIP-132, OWI-GP7611, & ADCP surface & pressure tracking w/ instrument @ 1-m elev.
Hs (m)
3
2.5
2
1.5
1
0.5
0
12/11
12/12
12/13
12/14
12/15
12/16
12/17
12/18
12/19
12/20
12/21
A6-surf
A1-press
CDIP-132
OWI-GP7611

REFERENCES

Churchill, J. H., Plueddemann, A. J., & Faluotico, S. M. (2006). *Extracting wind sea and swell from directional wave spectra derived from a bottom-mounted ADCP*. Retrieved from

Dally, W. R., & Osiecki, D. A. (2004). *Incorporating Bottom Friction into STWAVE*. Retrieved from 1010 Atlantic Street, Suite C, Melbourne Beach, Florida 3295:

Dally, W. R., & Osiecki, D. A. (2006). *Development & validation of hindcast-driven nearshore wave information.* Paper presented at the Proceedings of the 9th International Workshop on Wave Hindcasting and Forecasting.

Dean, R. G., & Dalrymple, R. A. (1991). *Water wave mechanics for engineers and scientists* (Vol. 2): world scientific publishing company.

Dean, R. G., & Dalrymple, R. A. (2004). *Coastal processes with engineering applications*: Cambridge University Press.

Gallagher, S., Tiron, R., & Dias, F. (2014). A long-term nearshore wave hindcast for Ireland: Atlantic and Irish Sea coasts (1979–2012). *Ocean Dynamics, 64*(8), 1163-1180.

Golden, S. (2022). Surfer 8 contouring and 3D surface mapping for scientists and engineers user's guide. Golden Software. *Inc., Colorado USA, www. goldensoftware. com*.

Gordon, R. L. (1996). Acoustic Doppler current profiler-Principles of operation: A practical primer. *Rd Instruments, 54*, 54.

Howell, G. (1980). Florida coastal data network. *Coastal Engineering Proceedings*(17), 25-25.

Instruments, R. (2008). WavesMon User's Guide & Quick Start (ICN078).

Instruments, R. D. (1996). Acoustic Doppler current profiler principles of operation: A practical primer. *RD Instruments, 1*.

Janssen, G., Kleef, H., Mulder, S., & Tydeman, P. (2008). Pilot assessment of depth related distribution of macrofauna in surf zone along Dutch coast and its implications for coastal management. *Marine ecology, 29*, 186-194.

Leadon, M. E., Dally, W. R., & Osiecki, D. A. (2004). *The Florida coastal forcing project.* Paper presented at the Proceedings of the 17th National Conference on Beach Preservation Association.

Massey, T. C., Anderson, M. E., Smith, J. M., Gomez, J. M., & Jones, R. (2011). STWAVE: Steady-state spectral wave model user's manual for STWAVE, Version 6.0.

Nielsen, P. (1992). *Coastal bottom boundary layers and sediment transport* (Vol. 4): World scientific.

NOAA. Retrieved from https://www.ndbc.noaa.gov/station_page.php?station=41112

oceanweather. (2006). *Global Reanalysis of Ocean Waves Fine Atlantic Basin (GROW-FAB)*. Retrieved from

oceanweather. (2022). GROW-FINE U.S. East Coast: Global Reanalysis of Ocean Waves – U.S. East Coast.

Pena, S. (2019). *Development, Validation, and Utilization, of a Long-term Nearshore Synthetic Wave Record*: University of North Florida.

Ryan, W. B., Carbotte, S. M., Coplan, J. O., O'Hara, S., Melkonian, A., Arko, R., . . . Nitsche, F. (2009). Global multi-resolution topography synthesis. *Geochemistry, Geophysics, Geosystems, 10*(3).

Simpson, M. R. (2001). *Discharge measurements using a broad-band acoustic Doppler current profiler*: US Department of the Interior, US Geological Survey Reston, CA, USA.

Smith, J. M., Sherlock, A. R., & Resio, D. T. (2001). *STWAVE: Steady-state spectral wave model user's manual for STWAVE, Version 3.0*. Retrieved from

Van der Westhuysen, A. (2012). *Modeling nearshore wave processes.* Paper presented at the ECWMF Workshop on Ocean Waves, European Centre for medium-range weather forecasts, Reading.

Woolf, D., & Mcilvenny, J. (2011). Data Sources for Offshore Renewable Energy.